RESPONSE AND FAILURE ANALYSIS OF A GRAPHITE-EPOXY LAMINATE CONTAINING TERMINATING INTERNAL PLIES

by

Brian Lee Kemp

Thesis submitted to the Faculty of the

Virginia Polytechnic Institute and State University

in partial fulfillment of the requirements for the degree of

MASTER OF SCIENCE

in

Aerospace and Ocean Engineering

APPROVED:

E. R. Johnson, Chairman

R. T. Haftka

C. T. Herakovich

July 1985

Blacksburg, Virginia

ACKNOWLEDGEMENTS

I wish to thank my family and faculty chairman, Dr. Johnson, for their support, encouragement and ideas over the course of completing this thesis.

I also would like to thank the Computing Center Staff for their patience with my tiring questions regarding the University's available software.

I would like to recognize Dr. J. H. Starnes, Jr. of NASA Langley Research Center and thank him for the sample specimens and questions regarding the problem.

Especially, I wish to thank Suzanne Remeikis for typing this manuscript through its drafting stages.

TABLE OF CONTENTS

Page

ACKNOWLEDGEMENTS ii

TABLE OF CONTENTS iii

LIST OF TABLES iv

LIST OF FIGURES v

Chapter

1 INTRODUCTION 1

1.1 Literature Review 2

1.2 Objectives of this Study 7

2 PROBLEM FORMULATION 10

2.1 Geometric Considerations 10

2.2 Generalized Plane Deformation 15

2.3 Finite Element Discretization 19

2.4 Loading Methodology and Boundary Conditions 25

2.5 Mesh Selections 29

2.6 Failure Analysis 34

3 NUMERICAL RESULTS 36

3.1 Axial Strain Variation Through the Laminate Thickness 37

3.2 Transverse (Interlaminar) Shear Stress Variation 41

3.3 Interlaminar Normal Stress Variation 49

3.4 Failure Predictions 53

4 DISCUSSION AND CONCLUSIONS 61

REFERENCES 65

APPENDIX A Comparison of Finite Element to Exact Elasticity ... 67

VITA 70

LIST OF TABLES

Tables — Page

1. Material Property Data.................................. 9

2. Quadratic Interpolation Polynomials.................... 21

3. Maximum Magnitudes of the Normalized Interlaminar....... 48
   Shear Stress τ_{xz}/σ_∞, and the Axial Distances for Stress Dissipation

4. Applied Axial Strain for Resin Failure.................. 55

5. Tensile Axial Strain for Intralamina Failure........... 57

6. Compressive Axial Strain for Intralamina Failure........ 59

LIST OF FIGURES

Figures Page

1. Typical cross section of a dropped ply.................. 3

2. Various widely-investigated geometries.................. 5

3. Microphotograph of $((+45/-45/0/90)_s0_D)_s)$ 11
dropped ply transition from 18 plies to 16 plies

4. Microphotograph of $((+45/-45/0/90)_s$..................... 12
dropped ply transition from 24 plies to 16 plies

5. Idealized model and variable notation.................. 13

6. Isoparametric mappings of variables..................... 22

7. Crude finite element mesh of dropped ply 30
transition from 3 plies to 2 plies, with nonsymetric boundary conditions

8. Typical finite element mesh............................. 33

9. Axial strain variation through thickness for............ 38
symmetric case

10. Axial strain variation through thickness for 39
nonsymmetric case

11. Interlaminar shear stress variation through 42
thickness for symmetric case

12. Interlaminar shear stress variation through 43
thickness for nonsymmetric case

13. Interlaminar shear stress variation along axis.......... 46
for symmetric case

14. Interlaminar shear stress variation along axis 47
for nonsymmetric case

15. Interlaminar normal stress variation through 50
thickness for symmetric case

16. Interlaminar normal stress variation through............ 51
thickness for nonsymmetric case

17. Interlaminar normal stress variation along axis......... 52

CHAPTER 1

INTRODUCTION

Research in fiber reinforced composite materials has enjoyed considerable popularity in recent years. High strength-to-weight and stiffness-to-weight ratios make structural applications of composite materials ideal in weight-sensitive structures. In the design of laminated filamentary composite structures, one of the most important considerations is the initiation and growth of transverse failure modes, i.e., delamination and transverse cracking. These failure modes are due to low strength and stiffness in the matrix dominated directions.

Composite materials are susceptible to the effects of stress concentrations which produce complex, three-dimensional deformations. Filamentary composite laminates are linear elastic and have low strain to failure; i.e., they behave in a brittle manner. As a brittle material system they would be expected to be more sensitive to stress concentrations. Discontinuities in geometry and material properties are common causes of stress concentrations. In this study the geometric discontinuity of a change in laminate thickness will be considered. A change in laminate thickness by terminating plies may be used to tailor the stiffness in a structural element. In designing laminated aircraft wing skins, for example, the laminate thickness could be thicker at the wing root, where increased thickness is beneficial, and thinner near the wing tip, where less stiffness is required. Also, increasing laminate thickness at holes and joints may be a means to increase strength at stress riser locations.

Two methods are available for increasing the thickness. In laminate fabrication, either the surface plies are added or terminated or the interior plies are added or terminated. Terminating or adding outer surface plies would create stress distributions between the additional plies and the remaining laminate which approximate the overlap region of an adhesively bonded joint. The exposed edge would be susceptible to delamination and reinforcement to prevent the overlay from disbonding would be required. Alternatively, internal plies can be terminated, and the remaining plies will encase the terminated ply from above and below. This will be referred to as a "dropped ply", see Figure 1. The dropped ply configuration avoids the adherend disbonding effects of step lapped joints present with terminating surface plies, but the dropped ply still acts as a through-the-thickness stress riser. The anticipated increase in load capacity created by thickening the laminate could be negated by the through-the-thickness stresses generated by the ply drop. Thus, it is important to examine the stress distributions in the vicinity of the ply drop and to predict the initiation of failure.

1.1 Literature Review

Recently the basic characteristics and geometric problems associated with the ply drop have been discussed [1-3] in an attempt to reduce the high stresses in joints. However, References 1-3 only point out that the ply drop is a source of interlaminar stress, no attempt is made to determine the stresses or deformations. A single reference

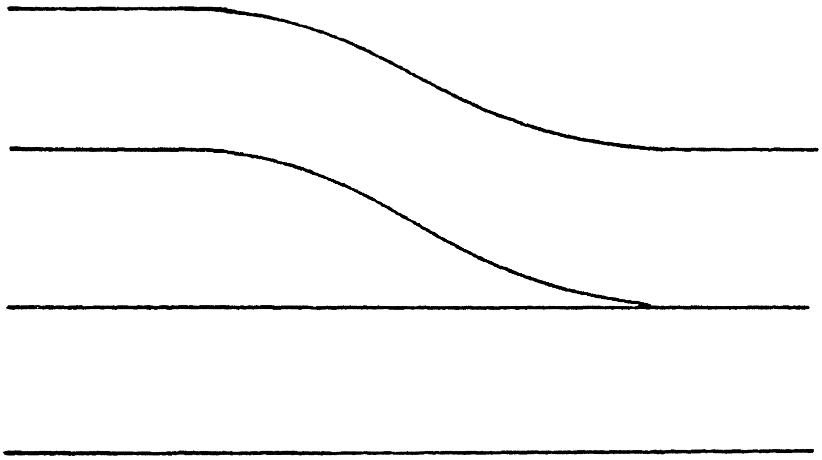

Fig. 1 Typical cross sectional view of a dropped ply.

pertaining to the analysis of the dropped ply configuration was found [4]. Adams, et. al., [4] investigated the reduction in longitudinal compression strength caused by dropping two 0^o plies in a thirty-ply $(0_{16}/(\pm 45)_5/90_4)$ graphite-epoxy (AS/3501-6) laminate. Experimental results were compared to a non-linear, three-dimensional finite element analysis and both indicated no degradation in compressive strength. Residual curing stresses were included in the modeling and found to be significant.

There are other geometric configurations which generate through-the-thickness stresses. Most notable is the classical "free-edge" problem in laminate elasticity (see Figure 2). In this problem, through-the-thickness stresses at the free edge of a finite-width composite laminate under uniform axial extension increase dramatically [5-7]. This problem mathematically reduces to a two-dimensional problem even though a fully three-dimensional stress and strain field exists. This class of elasticity problems is documented in Lekhnitskii [8]. References [5-7] have employed the finite element methods on this type of problem. A similar element to Reference 7 is used in this study to analyze the ply drop problem.

Also, the through-the-thickness stresses are generated in bonded lap joints (see Figure 2). Goland and Reisner [9] approached the analysis of single lap joints from two limiting cases. First the adhesive layer was assumed negligibly thin and was considered to have no effect on the joint flexibility. The alternative method models the bond layer to be sufficiently thick enough to be responsible for joint

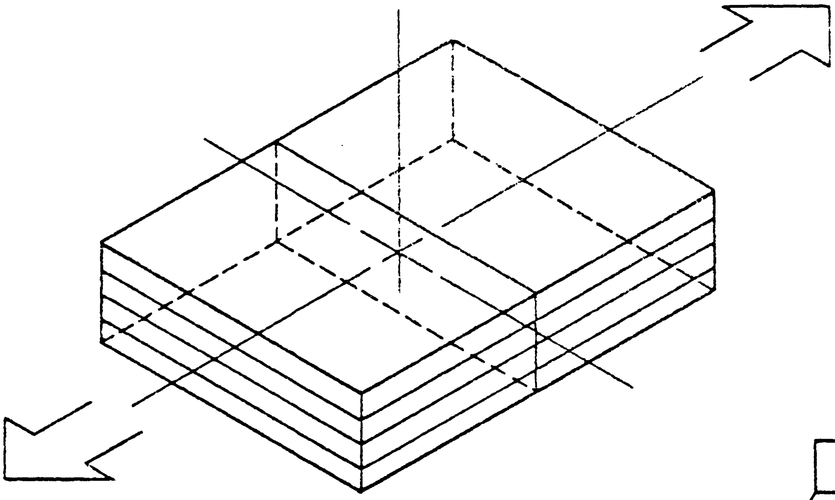

Uniform axial extension

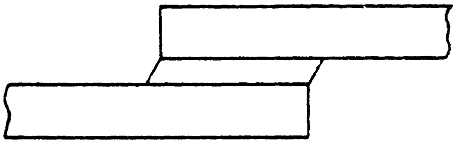

Single lap joint

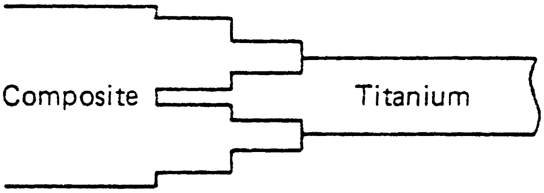

Stepped lap joint

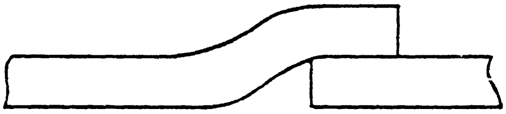

"Joggle-lap" joint

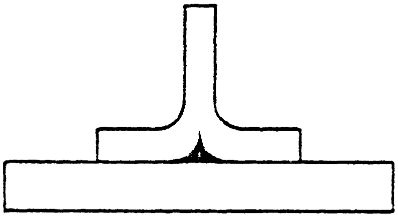

Spar-wingskin joint

Fig. 2 Various widely-investigated geometries.

flexibility. They determined that the critical regions are at the free edge adherend-adhesive interface.

In the analysis of stepped lap joints (see Figure 2), Hart-Smith [10] has shown that improved strength is achieved when the adhesive is critical, instead of the adherends. The titanium to composite step-lap joint investigated by Hart-Smith experienced interlaminar stress failures. Under fatigue loading, the joint fails due to higher than average shear load transfer at the ends of the steps. Hart-Smith proposed that the "optimum" design consisted of steps of sufficient length that the shear stress over the length step had decayed.

A joggle lap joint (see Figure 2) is typically used as a nonstructural joint for aerodynamic smoothness requirements [11]. The joint has low efficiency because of bending of the adherend due to eccentricty in the load path. For in-plane loads, the joint fails by peel stresses rather than by shear. The joggle lap joint is similar in geometry to the plies which will cover the drop section from above.

The above three joint studies demonstrate the importance of having sufficient distance along the joint in which to properly transfer the loads between adherends. The ply drop problem may be similarly interpreted as having a critical distance to transfer the loads to the added ply. In this critical distance the shear and normal (peel) stresses are large and may lead to failure by delamination.

As a final example on joint concepts the spar-wing skin joint also shown in Figure 2, was investigated by Cope and Pipes [12]. In this work a thin spar or stiffener was bonded to a wing skin and was parametrically studied to optimize out of plane strength. All the joining concepts which Cope and Pipes investigated considered an epoxy insert to fill the void created between the base of the spar and the wing skin. Loading perpendicular to the plate through the spar, a plane stress, finite element analysis predicted joint failure in the epoxy filled void. A larger epoxy insert resulted in a higher pull-off load. In the ply drop problem a pocket of pure resin (or "neat" resin) is present at the drop. This resin zone is similar to the wing skin joint in the sense that it can be considered as a design parameter to increase the effectiveness of the load transfer.

1.2 Objectives of this Study

The objectives of the present work are to determine the stress distributions in the vicinity of the ply drop and to predict the initiation of failure. Finite element techniques are used to approximate a solution to a generalized plane deformation analysis of the ply drop configuration subject to axial extension and compression. The work presented here investigates the characteristics of the stress distributions associated with variations in the geometric parameters.

Throughout this study, the material properties were held constant. No attempt was made to discern the effects of including non-linear or thermal variations in the stiffness or strength properties of the material. The lamina material is assumed to be T300/5208 unidirectional graphite-epoxy tape. Three-dimensional elastic stiffnesses for T300/5208 are required in the analysis, and the values reported by Knight [13] are used in this study. The strength values for T300/5208 used in the failure analysis are those values used by Herakovich [14]. These material properties are given in Table 1. Also, neat resin properties are required in this study, and the property values are listed in Table 1.

Table 1

Material Property Data

Material Properties of Unidirectional T300/5208

$20.0\ 10^6$ psi	E_1	Young's Modulus in the 1 direction
$1.4\ 10^6$ psi	E_2	Young's Modulus in the 2 direction
$1.4\ 10^6$ psi	E_3	Young's Modulus in the 3 direction
0.3	ν_{12}	Poisson's ratio $(-\varepsilon_2/\varepsilon_1)$
0.3	ν_{13}	Poisson's ratio $(-\varepsilon_3/\varepsilon_1)$
0.6	ν_{23}	Poisson's ratio $(-\varepsilon_3/\varepsilon_2)$
$0.8\ 10^6$ psi	G_{12}	Shear modulus in the 1-2 plane
$0.8\ 10^6$ psi	G_{13}	Shear modulus in the 1-3 plane
$0.6\ 10^6$ psi	G_{23}	Shear modulus in the 2-3 plane
218 ksi	$X_T = -X_C$	Fiber Direction Strength
5.9 ksi	$Y_T = Z_T$	Transverse Tensile Strength
-36 ksi	$Y_C = Z_C$	Transverse Compressive Strength
9.8 ksi	$S_{12} = S_{13} = S_{23}$	Shear strengths
$-1.9 \times 10^{-4}(\text{ksi})^{-2}$	$F_{12} = F_{13} = F_{23}$	Biaxial stress interaction coefficients

Material Properties of Neat Resin

$5.0\ 10^5$ psi	E_{resin}	Young's Modulus of resin
0.3	ν_{resin}	Resin Poisson's ratio
$2.78\ 10^5$ psi	G_{resin}	Shear modulus of resin
$5.40\ 10^3$ psi	X_{resin}	Maximum allowable absolute stress

CHAPTER 2

PROBLEM FORMULATION

2.1 Geometric Considerations

To properly model the ply drop problem, graphite epoxy specimens were fabricated with ply drops, and then cut to expose a through-the-thickness section in the vicinity of the drop. Microphotograph's of two laminates are shown in Figures 3 and 4. Figure 3 shows a laminate with two internal plies dropped and Figure 4 shows a laminate with eight plies dropped. Studying these actual specimens provided information on how to model the ply drop geometry.

Close inspection of the ends of dropped plies in the graphite-epoxy specimens showed a dark black triangular region of pure resin (see Figures 3 and 4). The size of the resin-rich region is large in comparison to the thicknesses of the individual orthotropic layers. Resin is the weakest constituent in composite structures and the resin pocket is located at the thickness change, where the internal load interaction will be severe. The pocket of resin cannot be neglected when modeling the problem. The parameteric study will investigate the effect of varying the size of this triangular region by increasing the height and length of the pure-resin region.

The idealized model shown in Figure 5 displays the notation used throughout this study. The right-handed Cartesian coordinate system shown in Figure 5 aligns the x, y, and z axes with the laminate length, width, and thickness, respectively. The laminate thickness is broken up

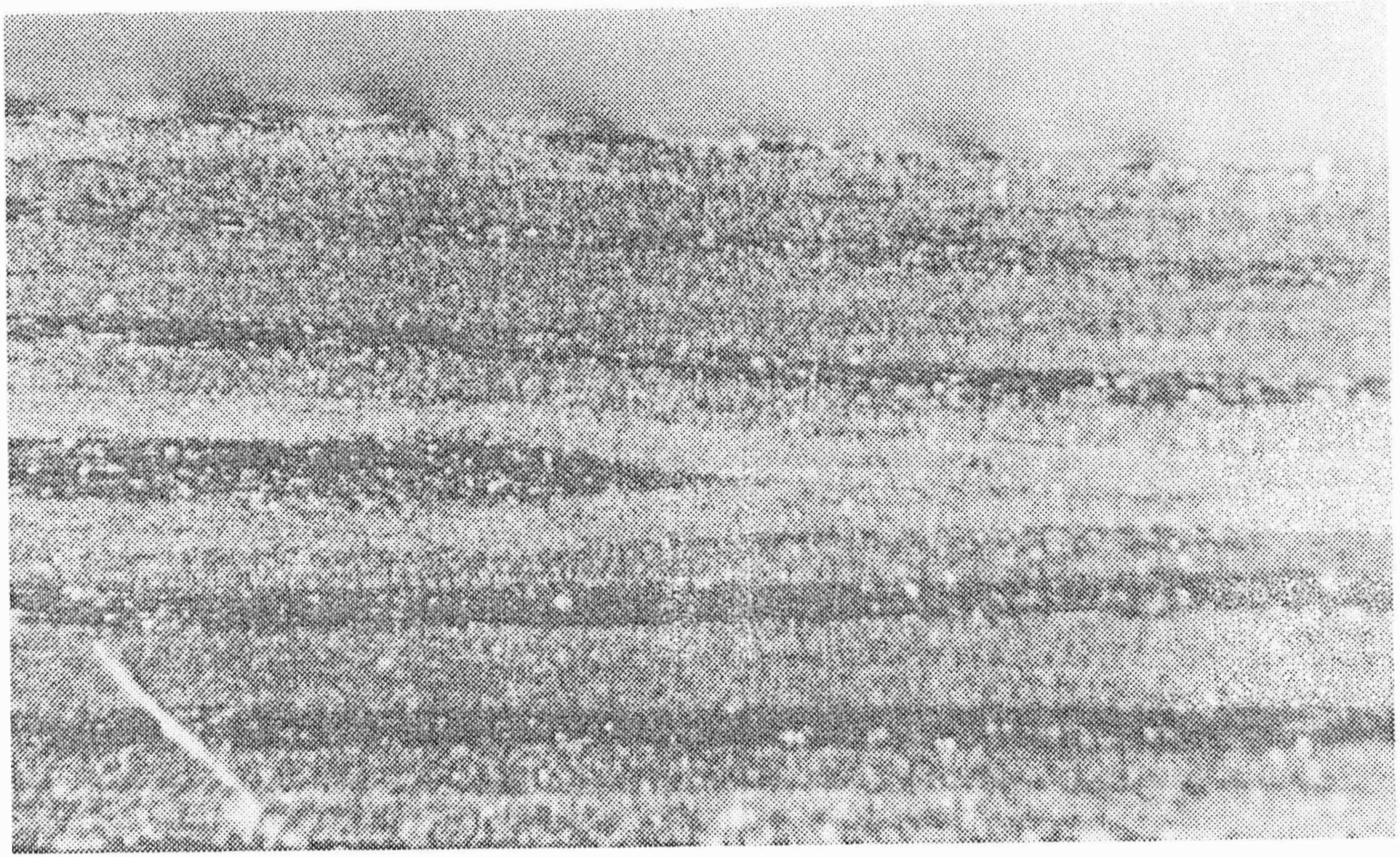

Fig. 3 Microphotograph of $((+45/-45/0/90)_S\ 0_D)_S$ dropped ply transition from 18 plies to 16 plies.

Fig. 4 Microphotograph of $((+45/-45/0/90)_S\ (+45/-45/0_2)_D)_S$ dropped ply transition from 24 plies to 16 plies.

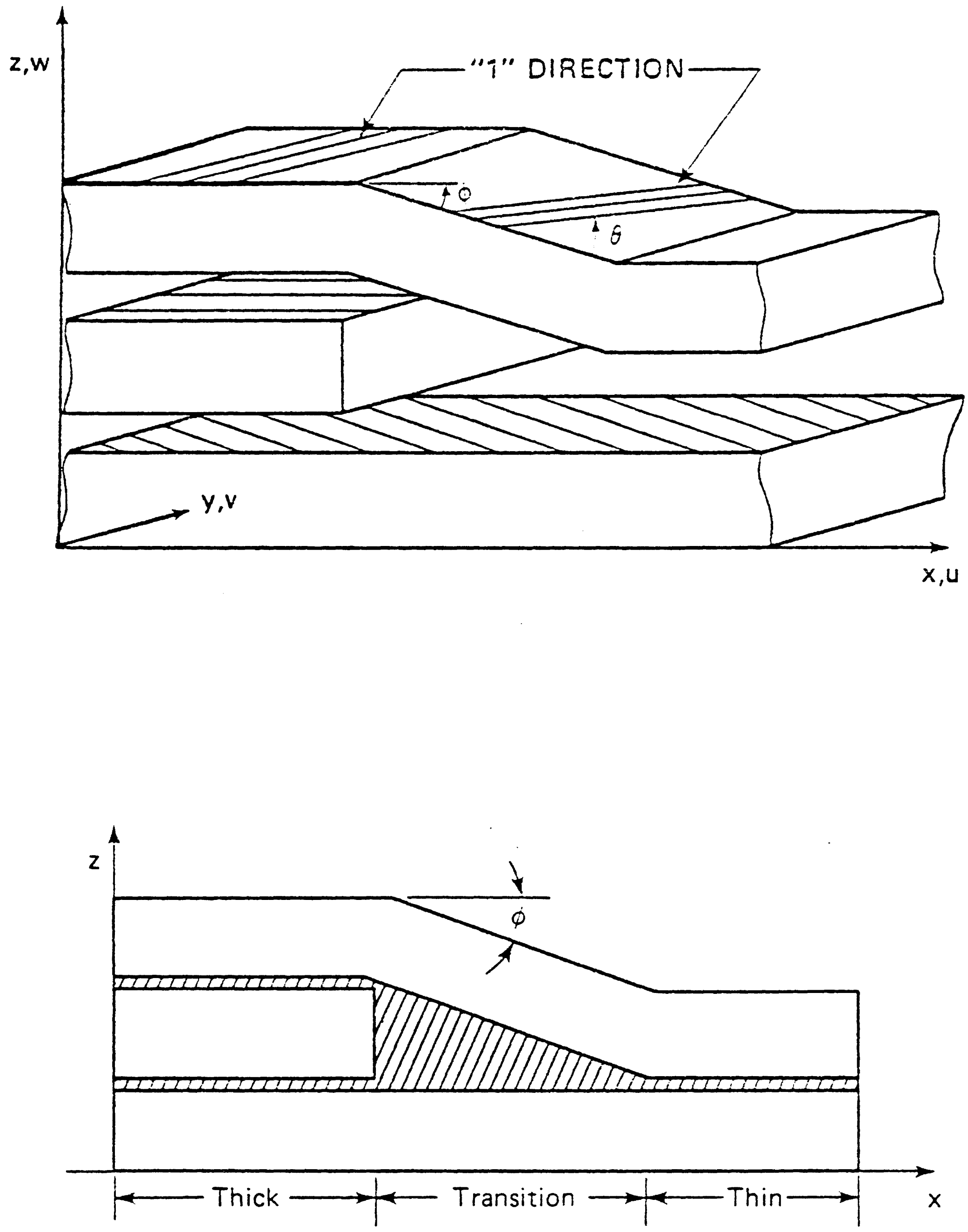

Fig. 5 Idealized model and variable notation.

into three sections: a "sub-laminate" below the drop, the dropped plies, and a "sub-laminate" above the drop. An individual ply has a thickness of h, while the total laminate thickness, including the dropped plies, is referenced as H_{TOT}. The x-axis, also referred to as the axial direction, is broken up into three sections: thick, transition, and thin. Finally, the width of the laminate is not specified except to assume that it is sufficiently wide such that edge effects in the y-direction are negligible.

In the thick and thin sections the fibers lie in a plane parallel to the x-y plane. The laminae are made of graphite-epoxy unidirectional tape with principal material directions 1, 2, and 3; where 1 is the fiber direction, 2 is orthogonal to 1 and in the plane of the tape, and 3 is orthogonal to 1 and 2 and is perpendicular to the plane of the unidirectional tape. The fiber direction is specified by the angle Θ, which is defined as a positive rotation (right-hand screw rule) about the normal to the fiber plane, and is measured from the axial direction to the local fiber direction. In the transition section, however, the fibers in the top "sub-laminate" cannot be described by a single rotation. The angle ϕ is defined as the rotation measured from the x-y plane to the inclined fiber plane of the material in the transition section. An angle ply will then be rotated by an additional angle Θ about the normal to the inclined fiber plane to obtain the principal material coordinate system (see Figure 5).

The ratio of length to height of the resin region will be referred to as the aspect ratio. Examining the sample specimens shown in Figures 3 and 4 an aspect ratio of three was assumed for the preliminary modeling. However, it is assumed that the size and shape of the triangular resin region can be varied by manufacturing processes. Recalling the spar-wing skin joint investigated by Cope and Pipes [12], an epoxy insert was manufactured to fill the void at the base which was created when the spar was co-cured to the wing skin. For the current configuration, the "void" caused by the dropped plies is filled by neat resin during the curing process. The effect of varying the aspect ratio was therefore included to determine its effects on the load transfer to the dropped plies.

2.2 Generalized Plane Deformation

In the transition section, the expected complex stress state warrants the use of a three-dimensional stress analysis. The potential energy of a three-dimensional elastic solid is composed of the volume integral of the strain engery density and the surface integral of the prescribed tractions along the boundary and is written

$$\begin{aligned} \Pi &= \iiint_{Vol} U_o \, dVol - W_e \\ &= \iiint_{Vol} 1/2 \, \{\sigma\}^T \{\varepsilon\} dx\, dydz - \iint_{S} \{u\}^T \{t\} \, dS \end{aligned} \tag{2.1}$$

where

U_o is the strain energy density

W_e is the external work done on the structure

$\{\sigma\}$ is the Cartesian stress vector

$$\{\sigma\}^T = \{\sigma_x \ \sigma_y \ \sigma_z \ \tau_{yz} \ \tau_{xz} \ \tau_{xy}\}$$

$\{\varepsilon\}$ is the Cartesian strain vector

$$\{\varepsilon\}^T = \{\varepsilon_x \ \varepsilon_y \ \varepsilon_z \ \gamma_{yz} \ \gamma_{xz} \ \gamma_{xy}\}$$

$\{u\}$ is the displacement vector of a material point, and

$\{t\}$ is the prescribed surface traction vector along the boundary.

In the surface integral for the external work, $\{t\}$ and $\{u\}$ are evaluated on the external surface (S). The surface traction vector, $\{t\}$, is related to the internal stresses at the boundary by Cauchy's formula. In a Cartesian coordinate system where ℓ, m, n are the direction cosines of the boundary normal, the external work is determined from the stress tensor matrix and is written as

$$W_e = \iint_S \{u\}^T\{t\}\, dS$$

$$= \iint_S \{u \ v \ w\} \begin{bmatrix} \sigma_x & \tau_{xy} & \tau_{xz} \\ \tau_{xy} & \sigma_y & \tau_{yz} \\ \tau_{xz} & \tau_{yz} & \sigma_z \end{bmatrix} \begin{Bmatrix} \ell \\ m \\ n \end{Bmatrix} dS \qquad (2.2)$$

The stress (σ) can be expressed in terms of the strain (ε) if the material is assumed to be linear elastic and that no deformations will remain when the structure is unloaded. Hooke's law can be expressed in general matrix form as

$$\{\sigma\} = [C]\{\varepsilon\} \tag{2.3}$$

where

[C] is the symmetric stiffness matrix

The stiffness matrix is a function of the material properties and, for orthotropic materials, the orientation of the local material coordinate system with respect to the structural coordinate system. The components of the stiffness matrix in terms of engineering constants in the principal material coordinate system may be obtained from Jones [1]. As previously stated, the principal axes are related to the global axes by two transformation rotations ϕ, Θ, (see Figure 5); where the proper order of the transformations is significant.

The stiffness matrix is expressed as the coordinate transformation from the principal material stiffness matrix (denoted by $[C_\ell]$) according to

$$[C\ ] = [T_y]^{-1}\ [T_z]^{-1}\ [C_\ell]\ [T_z]^{-T}\ [T_y]^{-T} \tag{2.4}$$

The transformation matrices $[T_y]$, $[T_z]$ are expressed as trigonometric functions of ϕ, Θ respectively. They are

$$[T_y] = \begin{bmatrix} m^2 & 0 & n^2 & 0 & -2mn & 0 \\ 0 & 1 & 0 & 0 & 0 & 0 \\ n^2 & 0 & m^2 & 0 & 2mn & 0 \\ 0 & 0 & 0 & m & 0 & n \\ mn & 0 & -mn & 0 & m^2-n^2 & 0 \\ 0 & 0 & 0 & -n & 0 & m \end{bmatrix} \qquad (2.5)$$

$$m = \cos\phi \qquad n = \sin\phi$$

$$[T_z] = \begin{bmatrix} m^2 & n^2 & 0 & 0 & 0 & 2mn \\ n^2 & m^2 & 0 & 0 & 0 & -2mn \\ 0 & 0 & 1 & 0 & 0 & 0 \\ 0 & 0 & 0 & m & -n & 0 \\ 0 & 0 & 0 & n & m & 0 \\ -mn & mn & 0 & 0 & 0 & m^2-n^2 \end{bmatrix} \qquad (2.6)$$

$$m = \cos\Theta \qquad n = \sin\Theta$$

Returning to the derivation of potential energy, Equation 2.3 may be substituted into Equation 2.1 to yield

$$\Pi = \int (1/2\ \{\varepsilon\}^T\ [C]\ \{\varepsilon\})\ dVol - \int (u)^T \{t\}\ d\ S \qquad (2.7)$$

The laminates considered here are assumed long enough in the y-direction such that stresses are independent of the y-coordinate. The special case in which the stresses are independent of y, and $\varepsilon_y = 0$ corresponds to Lekhnitskii's generalized plane deformation [8]. The strain-displacement relations when assuming the displacements are independent of y are

$$\underset{6\times 1}{\{\varepsilon\}} = \begin{Bmatrix} \varepsilon_x \\ \varepsilon_y \\ \varepsilon_z \\ \gamma_{yz} \\ \gamma_{xz} \\ \gamma_{xy} \end{Bmatrix} = \begin{Bmatrix} u,_x \\ v,_y \\ w,_z \\ v,_z + w,_y \\ u,_z + w,_x \\ u,_y + v,_x \end{Bmatrix} = \begin{Bmatrix} u,_x \\ 0 \\ w,_z \\ v,_z \\ u,_z + w,_x \\ v,_x \end{Bmatrix} \tag{2.8}$$

where u, v, w are displacements in the x, y, z directions, respectively, and the subscripted coordinate following the comma implies differentiation with respect to the coordinate.

2.3 Finite Element Discretization

The preceding derivation has been for a continuous system. In finite elements the energy terms must be approximated from discretized points, these points are referred to as nodal values. The finite element formulation approximates the displacements as

$$u = \sum_{i=1}^{n} N_i U_i \qquad v = \sum_{i=1}^{n} N_i V_i \qquad w = \sum_{i=1}^{n} N_i W_i \tag{2.9}$$

where U_i, V_i, W_i are the nodal displacements of the n-nodes and N_i are interpolation functions. The interpolation functions parametrically describe the shape of the displacement field. In this study, the same interpolation functions are used to describe the coordinates of the node points as

$$x = \sum_{i=1}^{n} N_i X_i \qquad z = \sum_{i=1}^{n} N_i Z_i \tag{2.10}$$

where X_i, Z_i are nodal coordinates (at a plane Y = constant). Since the same functions are used in both definitions, the element is defined as isoparametric. The interpolation functions chosen will be quadratic functions of the variables ξ,η, see Table 2. Figure 6 shows how the variables x,z are mapped into the variables ξ,η.

Since the independent variables are transformed via Equations (2.10), the derivatives with respect to x and z in Equation (2.8) are more readily expressed in the variables ξ,η by use of the chain rule. By using the chain rule, the Jacobian matrix [J] can be defined by

$$\begin{Bmatrix} \frac{\partial}{\partial \xi} \\ \frac{\partial}{\partial \eta} \end{Bmatrix} = \begin{bmatrix} \frac{\partial x}{\partial \xi} & \frac{\partial z}{\partial \xi} \\ \frac{\partial x}{\partial \eta} & \frac{\partial z}{\partial \eta} \end{bmatrix} \begin{Bmatrix} \frac{\partial}{\partial x} \\ \frac{\partial}{\partial z} \end{Bmatrix} = [J] \begin{Bmatrix} \frac{\partial}{\partial x} \\ \frac{\partial}{\partial z} \end{Bmatrix} \qquad (2.11)$$

Inverting the Jacobian allows the derivatives of x, z to be expressed as functions of the variables ξ,η and the nodal coordinates of the element. The strain $\{\varepsilon\}$ can now be written in terms of the nodal displacements as

$$\{\varepsilon\} = [B]\,\{q\} \qquad (2.12)$$

where

$$\{q\} = \{u_1\ v_1\ w_1\ u_2\ v_2\ w_2\ \ldots w_n\}$$

Table 2

Quadratic Interpolation Polynomials

$N_i=$	Triangular $n=6$	Quadrilateral $n=8$
1	$(1-\eta-\xi)\ (1-2\eta-2\xi)$	$-\frac{1}{4}(1-\xi)(1-\eta)(\xi+\eta+1)$
2	$\xi(2\xi-1)$	$\frac{1}{4}(1+\xi)(1-\eta)(\xi-n-1)$
3	$\eta(2\eta-1)$	$\frac{1}{4}(1+\xi)(1+\eta)(\xi+\eta-1)$
4	$4\xi(1-\xi-\eta)$	$\frac{1}{4}(1-\xi)(1+\eta)(\eta-\xi-1)$
5	$4\xi\eta$	$\frac{1}{2}(1-\xi^2)(1-\eta)$
6	$4\eta(1-\xi-\eta)$	$\frac{1}{2}(1-\eta^2)(1+\xi)$
7		$\frac{1}{2}(1-\xi^2)(1+\eta)$
8		$\frac{1}{2}(1-\eta^2)(1-\xi)$
where	$0\leqq\eta,\xi\leqq1$	$-1\leqq\eta,\xi\leqq1$

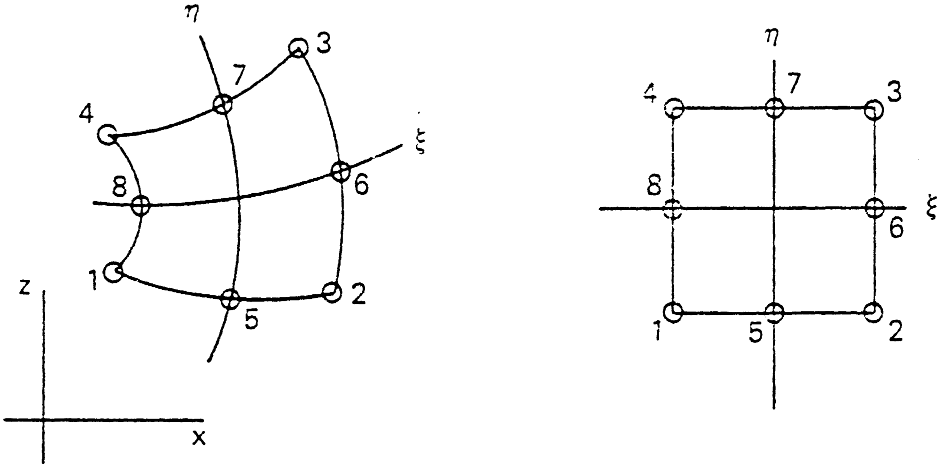

Quadrilateral element

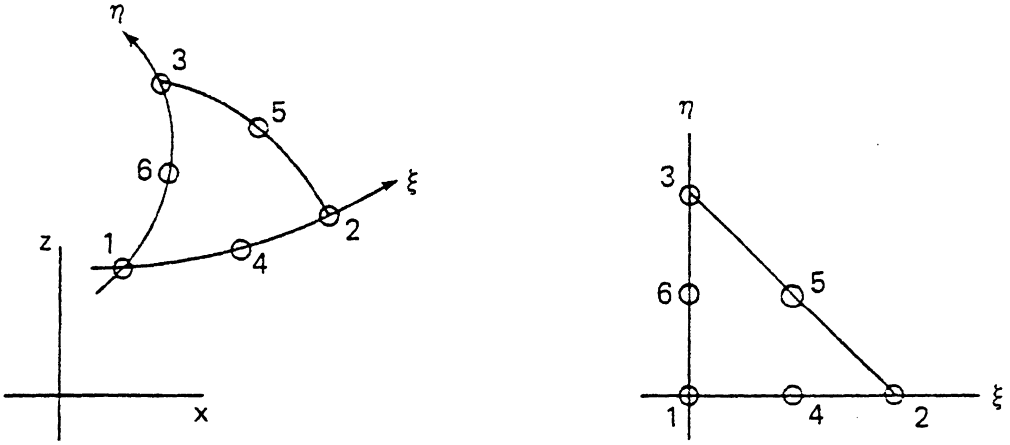

Triangular element

Fig. 6 Isoparametric mappings of variables.

and

$$[B] = [B_1\ B_2\ \ldots\ B_n]$$

$$[B_i] = \begin{bmatrix} \frac{\partial N_i}{\partial_x} & 0 & 0 \\ 0 & 0 & 0 \\ 0 & 0 & \frac{\partial N_i}{\partial z} \\ 0 & \frac{\partial N_i}{\partial z} & 0 \\ \frac{\partial N_i}{\partial z} & 0 & \frac{\partial N_i}{\partial x} \\ 0 & \frac{\partial N_i}{\partial x} & 0 \end{bmatrix}$$

The potential energy also requires a volume integration. The y-coordinate was eliminated from the integral and the Jacobian expresses the coordinate transformation. Therefore, the volume integral may be evaluated as

$$dVol = dy\ (dx\ dz) = \ell_y(\det|J|\ d\eta\ d\xi) \qquad (2.13)$$

where the integration in y is performed and evaluated on ℓ_y, the length in the y-direction.

Finally, the potential energy also requires an area integration (Equation 2.2). Again, since the problem has been assumed to be independent of the y-coordinate, the prescribed surface tractions must also be independent of y. The surface integral is evaluated as a line integral (ds) which is spatially uniform with y. The displacement vector in Equation 2.2 is expressed as the product of the nodal displacements and their respective shape functions (N_i). The integral is evaluated along all boundaries where tractions are specified. Substitition of Equations 2.12, 2.13 into the potential energy (Equation 2.7) yields

$$\Pi = \ell_y \left(\tfrac{1}{2} \{d\}^T [K] \{d\} - \{d\}^T \{F\} \right) \qquad (2.14)$$

where

$\{d\}$ is the vector of all nodal displacements

$[K] = \sum_{i=1}^{m} [k_i]^*$

$[k_i] = \iint_{A_i} [B]^T [C] [B] \det|J| \, d\eta \, d\xi$

$\{F\} = \sum_{i=1}^{m} \{f_i\}^*$

$\{f_i\} = \sum_{j=1}^{n} \int_S N_j^* \{t\} \, ds$

$\{t\}$ = is a vector of surface tractions

m = number of elements

n = number of nodes per element

$*$ indicates the vector is expanded so that nodal displacements or forces of elements are aligned with their global equivalent degree of freedom.

All of the integrations cited above are evaluated in the ξ, η plane, this is part of the versatility of the isoparametric formulation. Gaussian integration is used to determine the exact value of the integral by evaluating the integrand at so called "Gauss points" and summing these values with weighting factors [15]. For the problem stated here, the third order Gauss points were used to evaluate the integrals; three pre-determined locations along a unit length line determine the exact integral of a quintic polynomial.

The principle of minimum potential energy states that a static, conservative system is in equilibrium if its potential energy is a relative minimum [15]. Minimizing the potential energy (Equation 2.14) with respect to the discretized displacement vector $\{\underline{d}\}$ yields the standard finite element form

$$[K]\,\{\underline{d}\} = \{F\} \qquad (2.15)$$

The displacement vector $\{\underline{d}\}$ are the primary unknowns; the stresses are secondary unknowns which are computed from the displacements. Equation 2.15 is solved by inverting the global stiffness matrix [K] using either COLSOL [15] or OPTBLK [16]. Both of these are efficient mathematical FORTRAN programs using methods which use minimum core storage techniques to decompose a symmetric matrix in-core and out-of-core respectively. The results of an exact elasticity solution of an interlaminar stress problem [17] are compared to the finite element solution of the problem in Appendix A.

2.4 Loading Methodology and Boundary Conditions

It was decided to apply loads at $x = L$ which resulted in either a constant normal strain ε_x through the laminate thickness at $x = L$, or a linear distribution of ε_x through the thickness at $x = L$ that vanished at the middle surface. The former load case is pure axial extension or contraction, whereas the latter is pure bending. Unfortunately, the results for the pure bending case were not completed in this study, so that only the results for pure extension and contraction are given. To impose prescribed strains, the structure must be loaded with a force vector which will result in a predicted strain field. To determine the force vector, the stresses must be known at the point of load application.

In the thick section and the thin section, the structure resembles a flat laminate without stress risers. If it is assumed that classical lamination theory (CLT) [1,2] applies in the regions far away from the drop, then the strains are governed by a well defined set of hypotheses. CLT assumes that a line originally straight and perpendicular to the middle surface of the laminate remains straight and perpendicular to the middle surface when the laminate is extended and bent [1]. The foregoing assumption implies that the in-plane strains $(\varepsilon_x, \varepsilon_y, \gamma_{xy})$ vary linearly through the thickness of the laminate and can be written as

$$\begin{Bmatrix} \varepsilon_x \\ \varepsilon_y \\ \gamma_{xy} \end{Bmatrix} = \begin{Bmatrix} \bar{\varepsilon}_x \\ \bar{\varepsilon}_y \\ \bar{\gamma}_{xy} \end{Bmatrix} + z \begin{Bmatrix} \kappa_x \\ \kappa_y \\ \kappa_{xy} \end{Bmatrix} \tag{2.16}$$

where $\bar{\varepsilon}_x$, $\bar{\varepsilon}_y$, $\bar{\gamma}_{xy}$ are the strain of the midplane surface of the laminate and κ_x, κ_y, κ_{xy} are the curvatures of the midplane surface of the laminate.

In addition to the above assumptions on strain, the laminate is assumed to be free to contract from Poisson effects through the laminate thickness. A reduced stiffness matrix, [Q], is defined by eliminating ε_z variation from Hooke's law by setting $\sigma_z = 0$ and is written as

$$Q_{ij} = C_{ij} - \frac{C_{i3}C_{j3}}{C_{33}} \tag{2.17}$$

The above assumptions (Equations 2.16, 2.17) can be collected with the generalized deformation assumptions to explicitly determine the axial surface traction vector {t} (Equation 2.2). Assuming the laminate is supported axially in the thick section, then the surface traction vector which is applied axially to the right of the thin section is defined by

$$\{t\} = \begin{Bmatrix} \sigma_x \\ \tau_{xy} \\ \tau_{xz} \end{Bmatrix} = \begin{bmatrix} Q_{11} & Q_{16} & 0 \\ Q_{16} & Q_{66} & 0 \\ 0 & 0 & Q_{55} \end{bmatrix} \begin{Bmatrix} \bar{\varepsilon}_x + z\,\kappa_x \\ \bar{\gamma}_{xy} + z\,\kappa_{xy} \\ \gamma_{xz} \end{Bmatrix} \tag{2.18}$$

For uniform extension and contraction at x = L we prescribe $\bar{\varepsilon}_x = \varepsilon_{\text{applied}}$, $\bar{\gamma}_{xy} = \gamma_{xz} = \kappa_x = \kappa_{xy} = 0$ in Equation (2.18), where $\varepsilon_{\text{applied}}$ denotes the applied strain.

Because of the step in laminate height, applying forces in the thin section requires forces and moments in the thick section to maintain equilibrium. Calculating the stress resultants and maintaining force equilibrium will pre-determine the strains in the thick section as a function of the strain applied in the thin section.

The upper surface of the laminate is traction free. However, two separate conditions are assumed for the lower surface. In the nonsymmetric case, the lower surface is also traction free. Thus the load path is eccentric because of the change in height due to the dropped plies. The eccentricity results in a strain which varies linearly through the laminate thickness in the thick section for an applied uniform strain in the thin section. In the symmetric case, the lower surface is assumed to be a plane of symmetry. The load path is concentric and uniform applied strains in the thin section results in uniform strains in the thick section. However, the symmetry conditions on the lower surface doubles the laminate thickness and total number of plies dropped. The nonsymmetric case is applicable to an aircraft wing skin where one surface must remain flat, while the symmetric case may represent a stiffened region near a hole. The two cases are used to attempt to discern what effect the load path eccentricity will have on the ply drop.

The boundary conditions at $z = 0$ are determined by symmetry conditions. The z-axis is an axis of polar (or inversion) symmetry, which means that a 180^0 rotation of the laminate (geometry, material properties, boundary conditions, and load) about the z-axis brings the laminate into self-coincidence. Thus

$$\begin{aligned} u(x,y,z) &= -u(-x,-y,z) \\ v(x,y,z) &= -v(-x,-y,z) \\ w(x,y,z) &= w(-x,-y,z) \end{aligned} \tag{2.19}$$

and this symmetry implies $u = v = 0$ at $x = y = 0$. In addition, we have assumed that the displacements are independent of y, so that $u = v = 0$ in the entire y-z plane at $x = 0$. In the finite element model, then, the boundary conditions prescribed at $x = 0$ are $u = v = \tau_{xz} = 0$.

2.5 Mesh Selections

For the finite element analysis the element type, material constants, loads, and boundary conditions have all been decided. The final step before solving the problem is the grading of the finite element mesh. To achieve a finite element mesh which will solve the problem with a reasonable number of degrees of freedoms, a preliminary analysis was performed on the mesh shown in Figure 7. The problem modeled was a three ply laminate with a layup of $0^{\circ}/90^{\circ}/0^{\circ}$ where the 90° center ply was dropped to yield a two-ply 0° laminate. Each lamina was subdivided into two elements through the thickness. Including the midside nodes, there are five grid points through each lamina thickness.

The numerical results from this preliminary analysis served a many-fold purpose. Though not presented here, the results display the regions of highest stress. The rate of convergence of a finite element analysis is proportionate to the refinement of the mesh [15]. A highly refined mesh, particularly in areas of quickly changing stresses, can represent more precisely a rapid variation in stress or strain just as a curved line is represented better by shorter straight line segments than by longer segments. Consequently, mesh refinement was confined to regions of rapid variation as predicted from preliminary analysis.

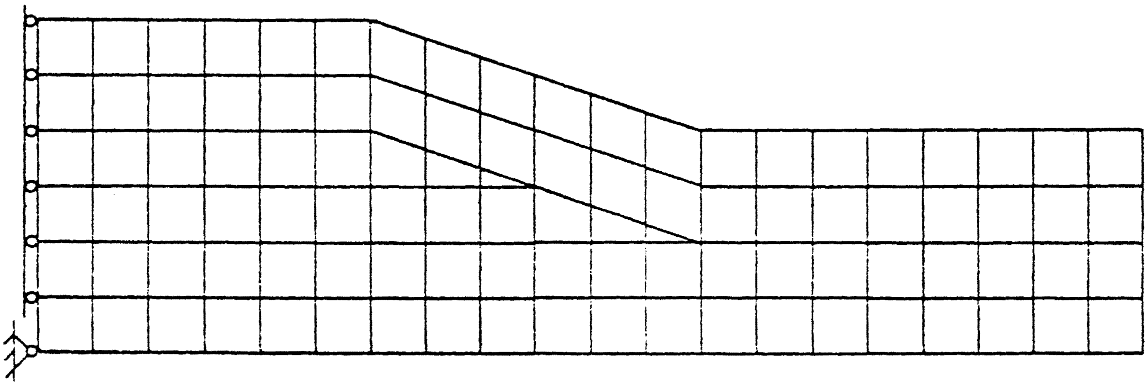

Fig. 7 Crude finite element mesh of dropped ply transition from 3 plies to 2 plies, with nonsymmetric boundary conditions.

Secondly, the preliminary analysis showed that a large portion of the load transfer to the dropped plies was through interlaminar shear and normal stresses at the ply drop. It was decided to model the interlaminar interfaces above and below the dropped plies as regions of pure resin with a thickness of 0.10h, where h denotes a lamina thickness. (The value for h used in the numerical results presented in Chapter 3 is 0.005 inches). Modeling the interlaminar interfaces as thin, resin-rich regions permitted the use of failure criteria commonly used in engineering. If a resin-rich interfacial region was not modeled, then a failure criterion for the interface between two perfectly bonded lamina must be postulated since such a criterion is not established. Postulating an interfacial criterion was avoided in this study by modeling a pure resin region between laminae, and assuming a common engineering failure criterion was applicable in this resin region. In addition, microphotographs of cross sections of laminates fabricated from graphite-epoxy undirectional tape show that regions of pure resin can exist between laminae with different orientations, and that these regions are on the order of two or three fiber diameters in thickness. Graphite fiber diameters are on the order of 0.00025 inches, so that a resin layer twice as thick corresponds to approximately ten-percent of a 0.005 inch lamina thickness.

Thirdly, the preliminary analysis verified the method of load application. When given ample distance for the stress risers to dissipate, the CLT results were recovered, and an axial normal strain which is uniform through the thickness occurred in the vicinity of the applied load. Finally, the preliminary analysis provided a reduced size data base which was used to evaluate various numerical techniques to interpret results. These numerical techniques also aided in determining how refined the mesh must be to reduce the discretization error.

For quadratic isoparametric elements, it is known that highest accuracy for secondary variables (stress, strain) is at the Guassian integration points [15] within the element field. Using the computed strains and stresses at the Gauss points and continuity conditions, the strains and stresses at other locations can be computed by interpolation. Continuity requires that the interlaminar stress components (σ_3, τ_{13},τ_{23}) and the in-plane strain components (ε_1, ε_2, γ_{12}) be continuous at lamina interfaces. Additionally, within subdivisions of a ply, all stress and strain components should be continuous.

The finite element mesh shown in Figure 8 is a typical mesh used in the analysis. The axial length is at least $3H_{TOT}$ in the thick section and 2 H_{TOT} in the thin section. At the termination point of the dropped ply, up to four elements are used through the lamina thickness to insure that the continuous components of stress and strain, as described above, did not vary wildly when interpolated to the element interfaces of any two adjacent elements. The largest problem solved used a total of 1833 nodes (with three degrees of freedom at each node) and 631 elements. In the numerical results presented, all of the data interpolation was performed with a three-dimensional grid routine available in Statictical Analysis System (SAS) [18] which estimated the

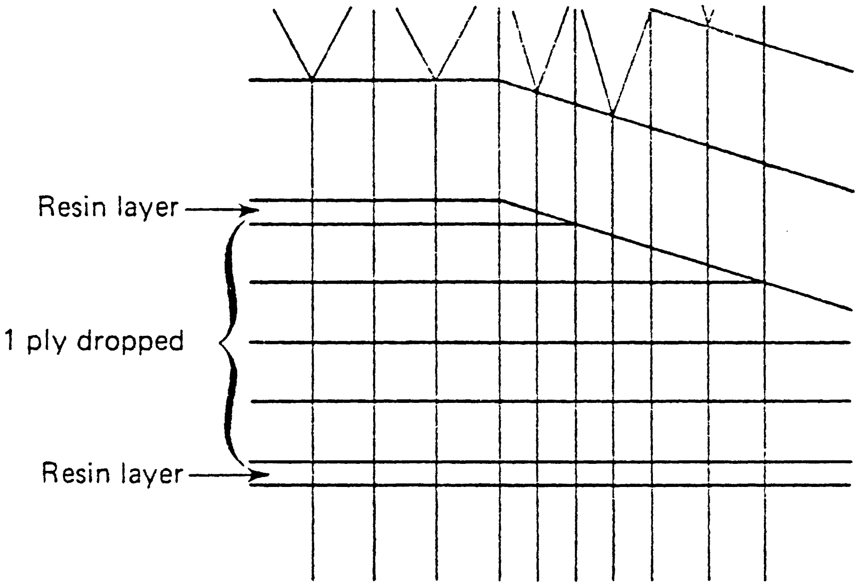

Blow up of mesh refinement at drop

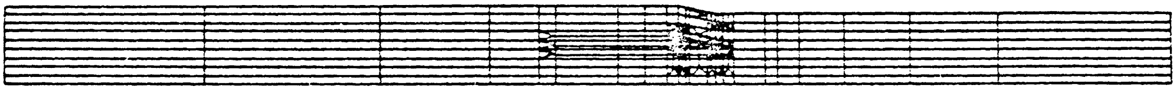

Fig. 8 Typical finite element mesh. All element shown have midside nodes.

variables and their derivatives from the eight closest neighboring Gauss points. Variations of stress and strain through the laminate thickness at the dropped plies is actually performed in the thick section just before the drop. This is done so that the interpolated variables are all from parallel fiber planes.

2.6 Failure Analysis

In addition to investigating the distributions of stress and strain, a prediction of the load carrying capability of the ply drop configuration is made. Two criteria are used to predict the strength of the ply drop. The criteria are applied at the Gaussian stations of the elements where stresses should have their highest accuracy, rather than extrapolating the stresses to the element edges.

In regions of pure resin, a maximum principal stress criterion is used to predict failure where the resin is assumed to behave linearly to failure. As shown in Table 1, the absolute magnitude of the largest principal stress in the resin must not exceed 5.4 ksi or the resin is assumed to fail. Since all six stress components are generally non-zero, the principal stresses are found by determining the eigenvalues of the stress tensor matrix. The resin is assumed to have the same strength in tension and compression, therefore extensional or compressive loading does not effect the magnitude of the failure load.

In the laminae, a three-dimensional Tsai-Wu criterion postulates the initiation of failure when

$$F_1\sigma_1 + F_2\sigma_2 + F_3\sigma_3 + F_{11}\sigma_1^2 + F_{22}\sigma_2^2 + F_{33}\sigma_3^2$$
$$+ F_{44}\tau_{23}^2 + F_{55}\tau_{13}^2 + F_{66}\tau_{12}^2 \quad (2.20)$$
$$+ 2F_{12}\sigma_1\sigma_2 + 2F_{13}\sigma_1\sigma_3 + 2F_{23}\sigma_2\sigma_3 = 1$$

where all stresses are in the principal material coordinate system, and the failure coefficients (F_1, F_2,,,F_{23}) are determined from the lamina strengths [1]. The strength values used by Herakovich, et. al [14] are assumed for this paper. In the laminate, the values of transverse compressive strengths are almost six times that of the extensional strengths. Therefore, the difference between extensional or compressional loading can have a great effect on the laminate strength. Both loading cases will be presented.

CHAPTER 3

NUMERICAL RESULTS

The results have been grouped into four classes; namely, there are two different layups, each with symmetric and nonsymmetric boundary conditions. The two layups chosen for this investigation are:

CASE 1: $(+45/-45/0/90/0_{nD}/90/0/-45/+45)$

CASE 2: $(0/90/+45/-45/0_{nD}/-45/+45/0/90)$

where in the subscript nD the 'n' denotes the number of dropped 0^{o}-plies. In the thick and thin regions the laminate is symmetric with respect to its mid-plane, therefore the stiffness matrix has no coupling between extension and bending. Also the two laminates (case 1 and case 2) have the same extensional stiffness characteristics, but different bending stiffnesses.

The number of 0^{o}-plies which are dropped determines the height of the resin zone, and either 1-, 2-, or 3-plies dropped are considered in this study. For a given number of dropped plies, the length of the resin zone was varied such that the aspect ratio ranges over 3, 4, 5 and 6. Since the numerical results for this parametric study are extensive (96 separate analyses in all), the results are presented from the response of a single configuration and deviations in the results due to different parameter values are addressed in the discussion. The configuration chosen, unless stated otherwise, as "typical" was a case 1 layup with three plies dropped and an aspect ratio of three. The results presented for laminate response are the axial strain distribution, and interlaminar shear and normal stress distributions. After presenting laminate response, the failure predictions are discussed.

3.1 Axial Strain Variation Through the Laminate Thickness

The structure is loaded with a uniform axial strain in the far field and the axial strain distribution exemplifies the effect of the ply drop. The axial strain is the dominate contributor to the axial stress in the stress-strain law, however, the material heterogeneity causes the axial stress to be discontinuous at ply interfaces. Therefore, since the axial strain is continuous across ply interfaces it is a better indicator of axial load conditions. Figures 9 and 10 present the variation of axial strain (normalized by applied strain in thin section) through the laminate thickness at four axial stations. Figure 9 presents results for the symmetric boundary conditions, while Figure 10 presents nonsymmetric results. In both cases note the linear variations through the laminate at points A and D. The vertical line at point D validates the procedure used in Section 2.4 to obtain a uniform far field axial strain. The vertical and sloping straight lines in Figures 9 and 10, respectively, are the predicted strains from CLT for the added stiffness of the dropped plies.

The through-the-thickness distributions in axial strain as the drop is approached from the thick section shows the severity of the ply

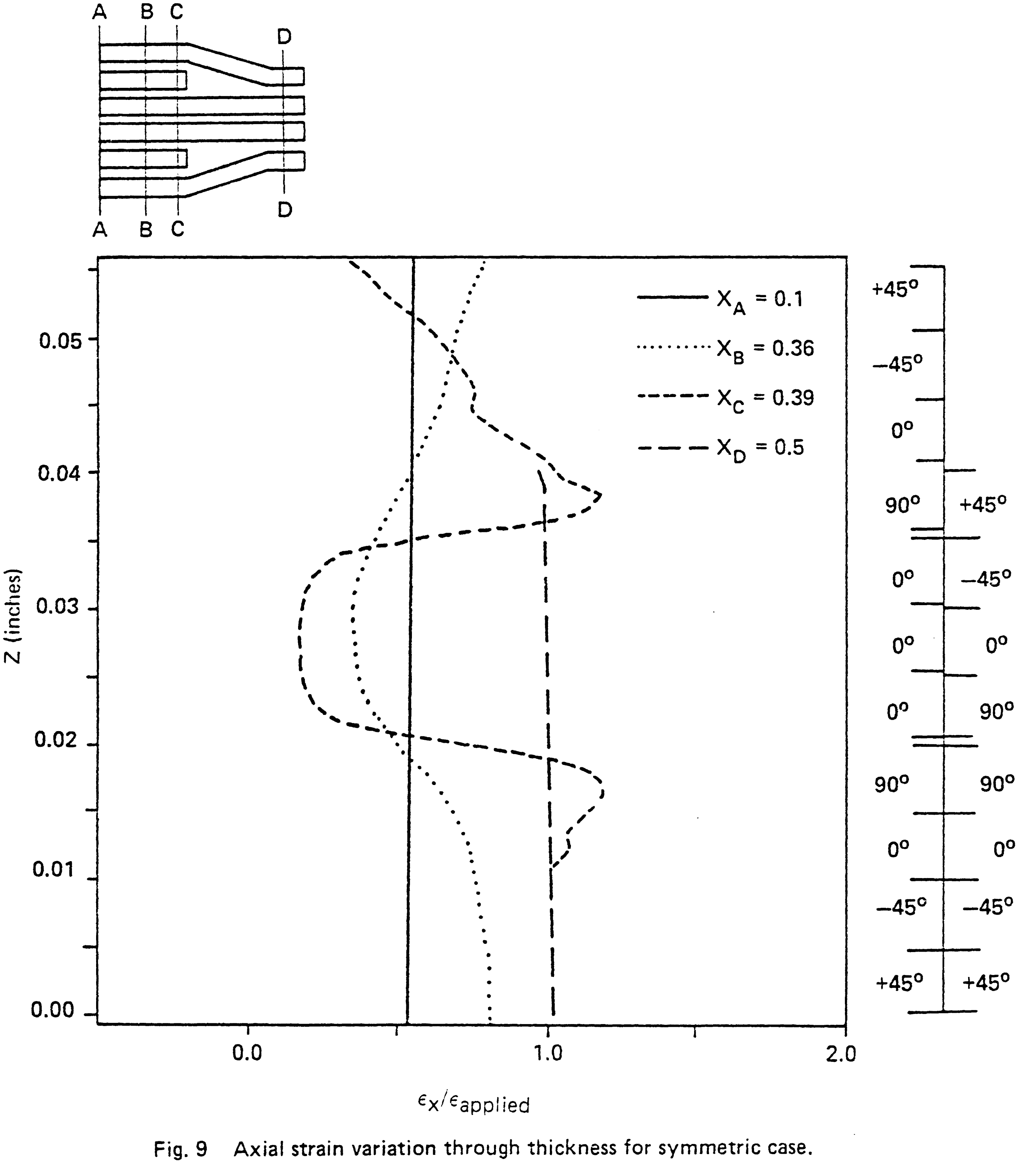

Fig. 9 Axial strain variation through thickness for symmetric case.

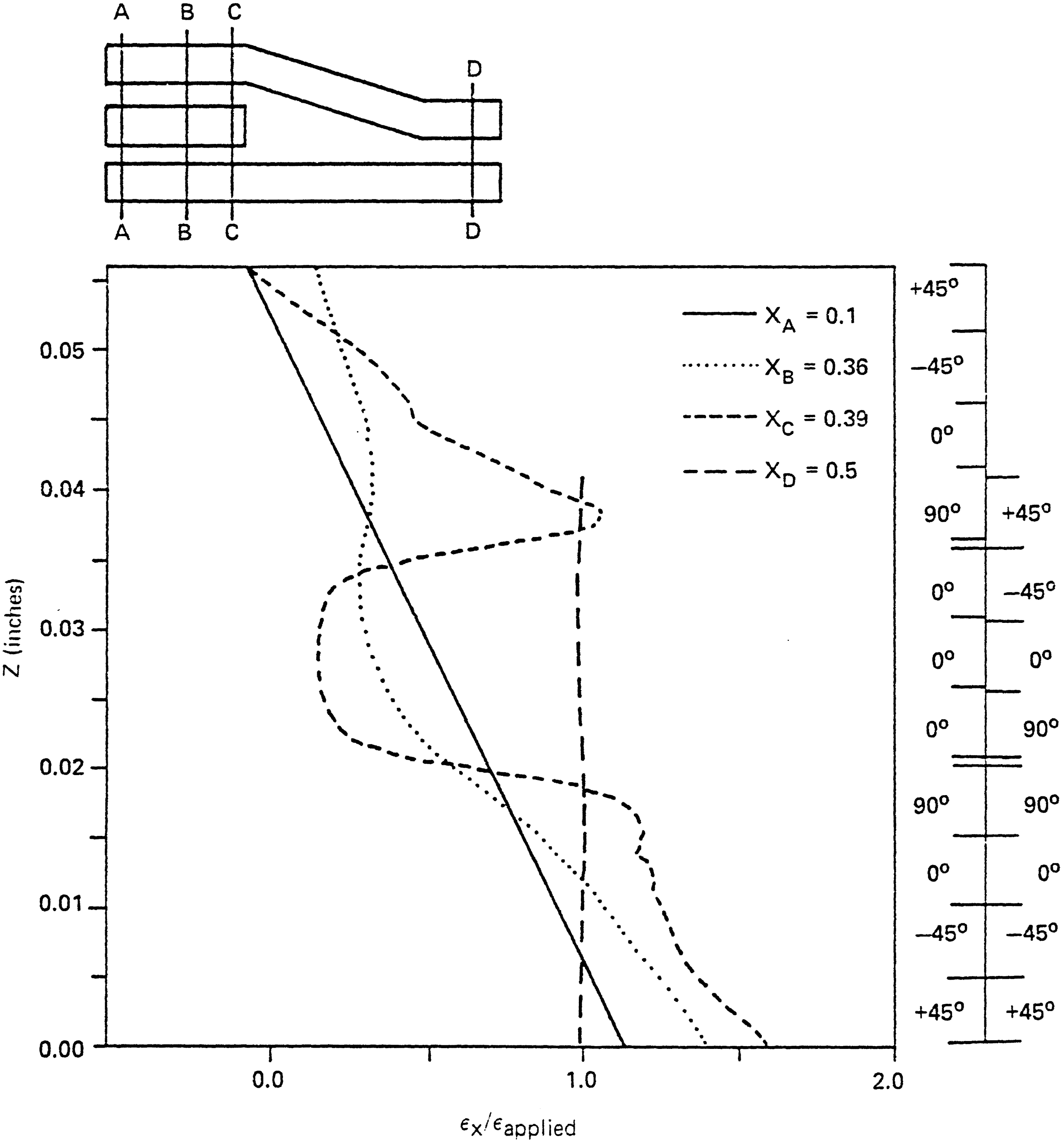

Fig. 10 Axial strain variation through thickness for non-symmetric case.

drop. Little load can be transferred through the fiber ends of the dropped plies from the resin. At point B, which is seven lamina thickness before the drop, there is a reduction of strain in the dropped plies. At point C, just prior to the drop, the axial strain in the dropped plies is approaching zero. In both the symmetric and nonsymmetric boundary cases, a local maximum in axial strain occurs in the ply just above the drop, and then the axial strain decreases almost linearly with increasing values of z. The nearly linear variation in axial strain at the drop in the outer plies indicates there is a significant amount of bending in the plies above the drop, even in the symmetric case.

In the drop ply laminate, there is also axial load carried in the plies below the drop, as shown by the non-zero axial strain in Figures 9 and 10. Again, the ply adjacent to the dropped ply (this time just below the drop) contains a local maximum at the termination point. However, in the remaining plies below the drop, the variation of strain resembles the CLT response. In both layup cases and symmetric or nonsymmetric conditions, the strain distribution in the lower plies has nearly the same slope as CLT, but with higher average values. Of particular concern, however, is the magnitude of axial strain at the lower surface of the nonsymmetric case. The outer ply experiences strains one and one-half times the applied strain.

For a fewer number of plies dropped, the peak values in the axial strain in the upper plies at the drop increase. This appears to be a result of less eccentricity in the load path. Also for a fewer number of dropped plies, the slope of the through-the-thickness distribution in axial strain becomes more vertical. Thus, the upper plies carry more axial load at the drop for a fewer number of dropped plies, and the axial bending moment in the upper plies is reduced. When increasing the aspect ratio of the resin pocket, the only significant variation seen in the axial strain occurs in the upper plies at the drop. As the aspect ratio is increased, the slope of the strain distribution is more vertical in the outer plies, implying the local bending moment in these outer plies is reduced.

When changing over to the case 2 laminate, all the above observations hold true. Additionally, there is a greater amount of strain carried in the plies adjacent to the drop. The case 2 laminate, however, also has higher stiffnesses in the adjacent plies (45^{o} plies rather than 90^{o}-plies), which means more axial load is being carried in the plies adjacent to the dropped plies.

3.2 Transverse (Interlaminar) Shear Stress Variation

Since a moment which varies rapidly with axial position has been determined to exist locally in the plies above the drop, in both the symmetric and nonsymmetric cases, the transverse shear stresses are likely to have significant magnitudes in these upper plies. Figures 11 and 12 show the variation of transverse (interlaminar) shear stress through the laminate thickness for the symmetric and nonsymmetric conditions, respectively.

These stresses, and the stresses in all the remaining figures, are normalized by the stress applied to the resin at the thin section (this stress is denoted as σ_{∞}). For both conditions, again note that the

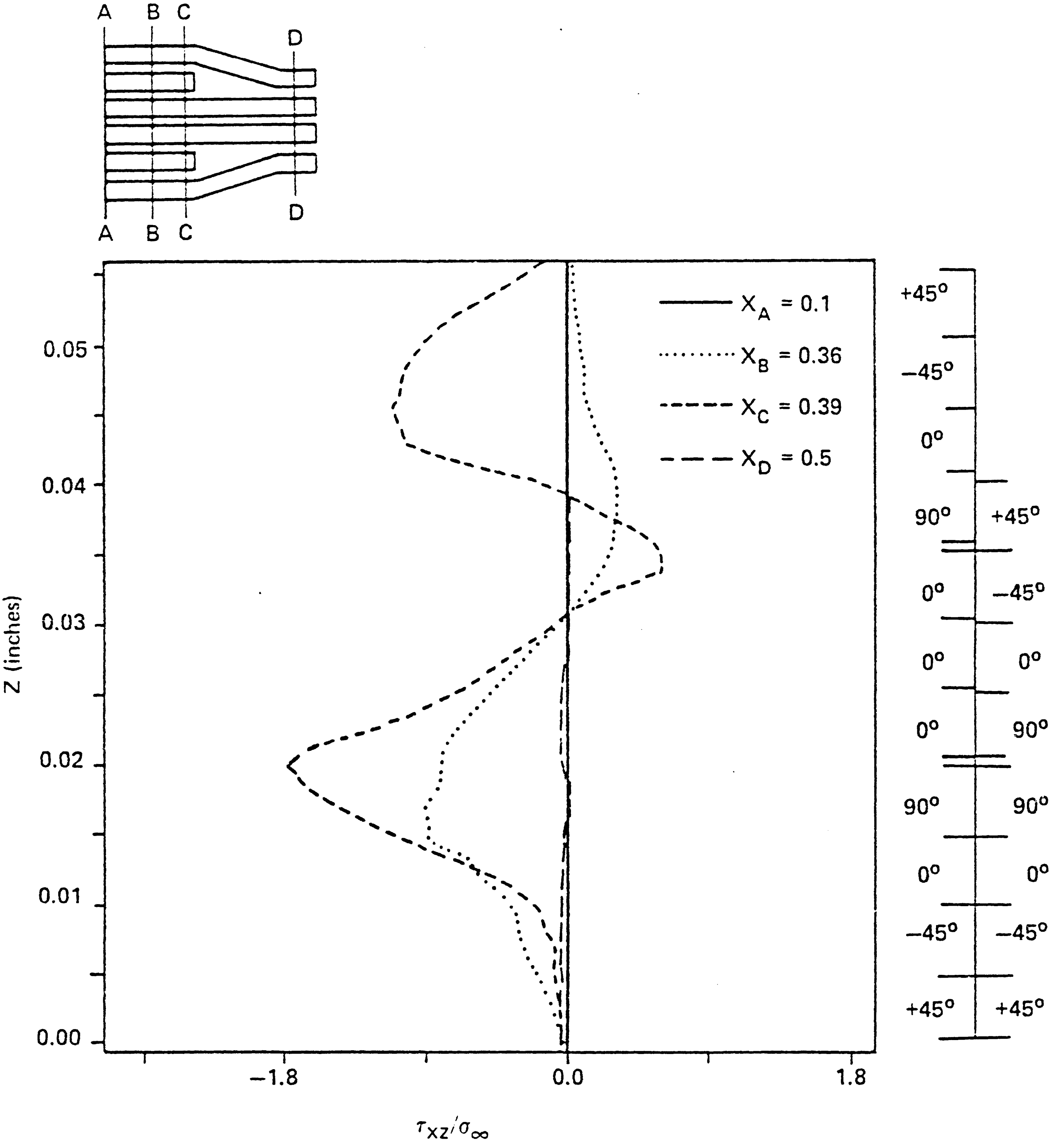

Fig. 11 Interlaminar shear stress variation through thickness for symmetric case.

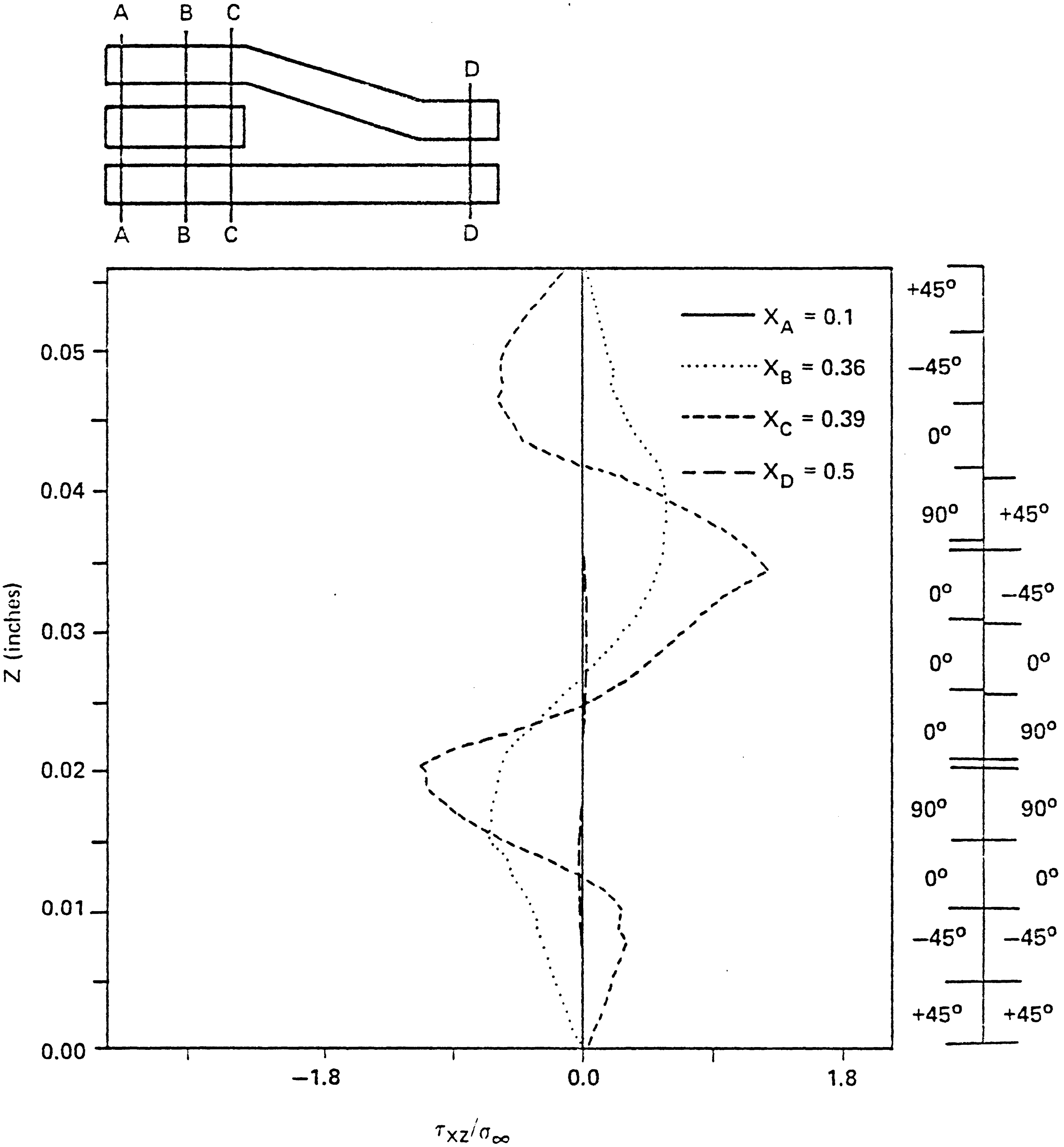

Fig. 12 Interlaminar shear stress variation through thickness for non-symmetric case.

initial assumptions of negligible transverse shear stress in regions far removed from the drop are verified. Approaching the drop in the thick section, the maximum magnitudes of the shear stress grows progressively larger going from points A to B to C. There are two important considerations to point out on these figures. First, the stress on the upper outer surface should be zero. However, this stress is being extrapolated from the element Gauss points, and is tending to zero without being forced to be identically zero. Second, to maintain equilibrium the area integral of the shear stress through the laminate thickness should be zero. This condition is satisfied exactly in the symmetric case since shear stresses will be of opposite sign below the x-axis. In the nonsymmetric case, this condition imposes an additional check on solution accuracy. Visual inspection of Figure 12 shows that points B and C meet this criterion.

Inspecting Figures 11 and 12, the shear stress in the regions near the ply interface have local peaks of different signs above and below the drop ply. For both symmetric and nonsymmetric conditions, there exists a region of negative shear stress in the upper plies at the drop. Proceeding in the negative x-direction from the drop, this region of negative shear in the upper plies decreases in magnitude and passes through zero to become positive before vanishing in the far field. The non-zero shear stress in the upper plies results from the axial variation in the axial moment in the upper plies, which exists because of load path eccentricity.

Looking closer at the peak shear stresses at the drop, the local maxima/minima occur very close to the resin-rich layers above and below the drop. Figures 13 and 14 show the axial variation of shear stress at the mid-height of the resin layers for the symmetric and nonsymmetric conditions, respectively. In addition to showing peak stresses at the ply termination point, a local maximum is also found at the axial location in the resin where the top "sub-laminate" rejoins with the bottom "sub-laminate". Although single components of stress are no indication of failure, the magnitude of the stresses at the ply drop were always found to be higher than the stresses at the rejoining point. In comparing the results from the symmetric and nonsymmetric conditions, the shear stresses in the resin layers decrease in magnitude in an exponential manner with increasing axial distance from the drop. In the upper resin interface for the symmetric condition, the variation in shear begins with a shallow exponential rise and then turns sharply with an increased exponential rise just prior to the drop (see Figure 11).

An important aspect of the shear stress distributions in the upper and lower resin layers is the axial distance from the drop where the shear stresses vanish. In the analysis of stepped-lap joints, Hart-Smith [10] has shown that the "optimal" length of a step is one which allows the shear stresses to vanish. Table 3 gives the axial distances for the interlaminar shear stresses to vanish for case 1 lay-up and symmetric boundary conditions. Although differences in the absolute maximum shear were found between the two boundary conditions, there was little difference in the distance required for the shear to

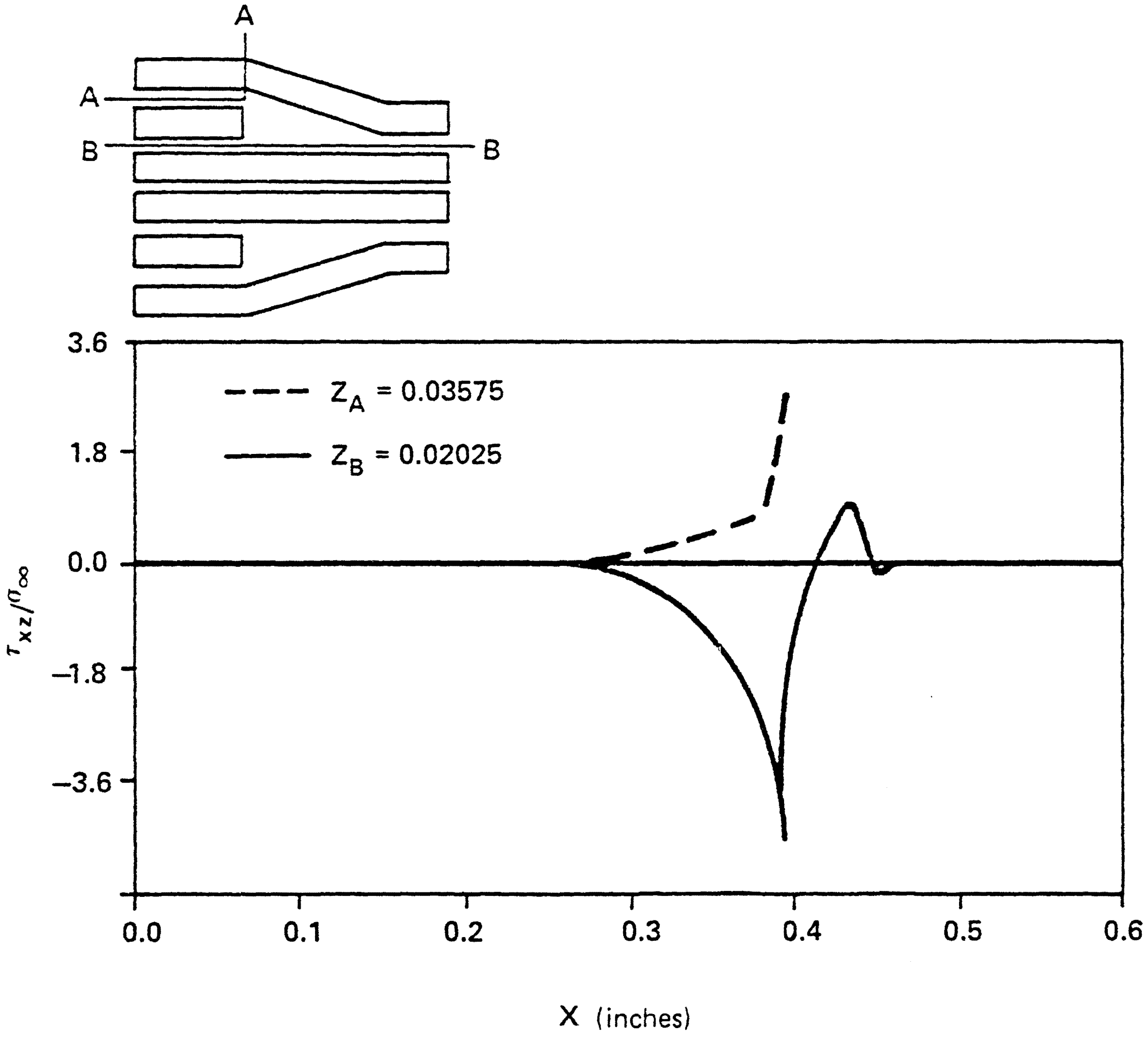

Fig. 13 Interlaminar shear stress variation along axis for symmetric case.

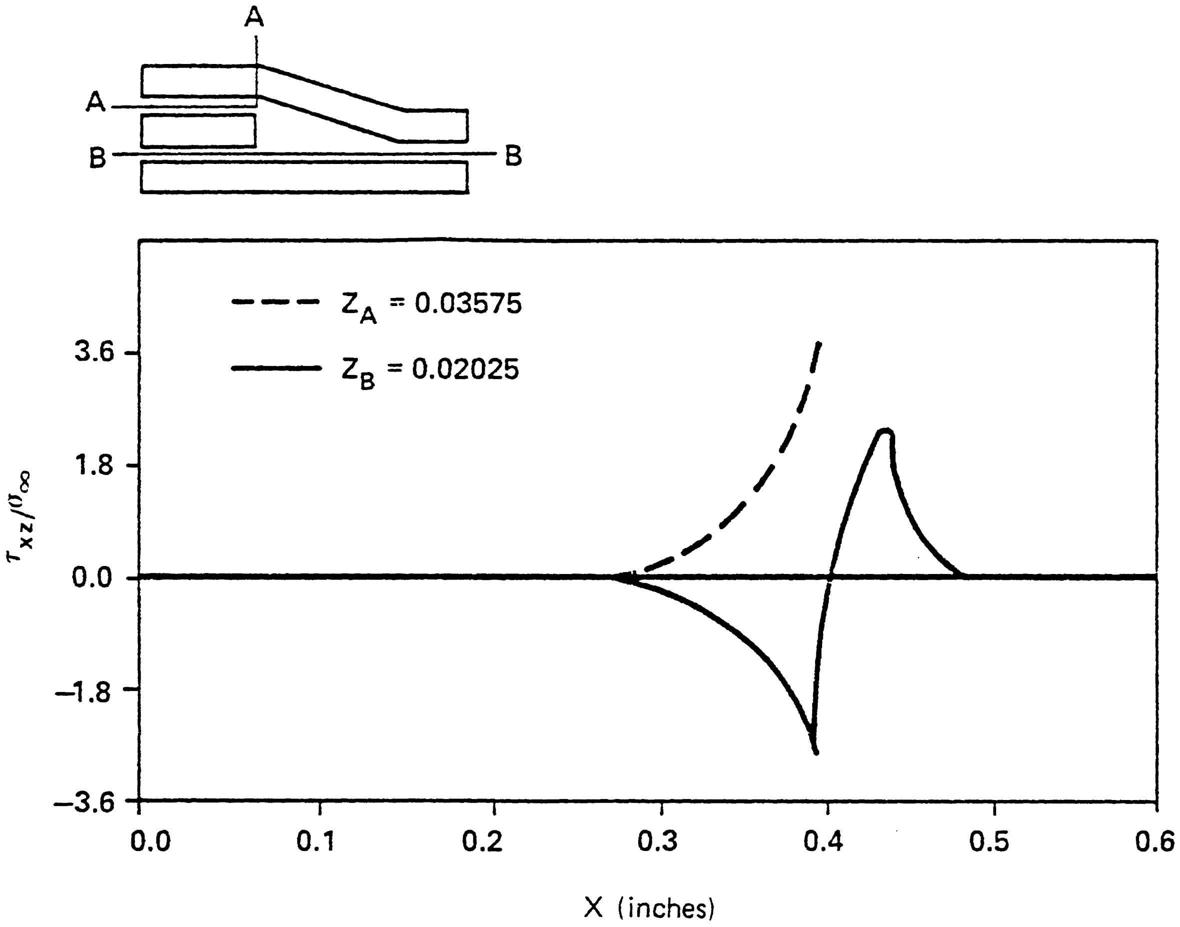

Fig. 14 Interlaminar shear stress variation along axis for non-symmetric case.

Table 3

Maximum Magnitudes of the Normalized Interlaminar Shear Stress $\tau_{xz}/\sigma_{\infty}$, and the Distances for Stress Dissipation

Aspect Ratio		n^{**}	
	1	2	3
3	3.20 (19h)	3.53 (27h)	3.89 (34h)
4	3.24 (18h)	3.64 (25h)	3.95 (33h)
5	3.23 (18h)	3.66 (26h)	3.86 (31h)
6	3.35 (18h)	3.73 (26h)	4.13 (32h)

---

[*] The results in this table are presented for the case 1 symmetric laminate. The maximum stress magnitudes occur in the lower interface at the ply drop-off, and are normalized by the axial normal stress in the resin (σ_{∞}) in the thin section at $x = L$. The axial distances for stress dissipation are given in parentheses in terms of lamina thickness h. The distance for stress dissipation is defined to be that distance at which the shear stress is reduced by 99% of its maximum magnitude.

[**] n equals the number of dropped 0^{o}-plies.

vanish. The effect of ply configuration was also small on the distance required for the shear stress to vanish, but the peak shear stresses were slightly higher for the case 2 lay-up.

In both lay-ups examined, the largest magnitude shear stress is a negative shear on the lower resin interface for symmetric conditions, and a positive shear on the upper interface for nonsymmetric conditions. Table 3 shows that the peak stresses are increased as the aspect ratio is increased from 3 to 6, and are increased as the number of plies dropped is increased. For increasing aspect ratio, however, the axial distance for the shear stress to vanish (hence referred to as shear distance) is increased only slightly. Significant increases in the shear distance result from an increase in the number of plies being dropped.

3.3 Interlaminar Normal Stress Variation

The final stress response investigated is the interlaminar normal stress. Looking first at the distribution through the laminate thickness, Figures 15 and 16 show negligible normal stress at axial locations A and D, and this agrees well with CLT assumptions. The stress-free condition on the upper surfaces is met at points B and C. Recall that in the symmetric case σ_z needs to be zero only on the top surface, since the lower surface is a plane of reflective symmetry. Again the resin layers at the drop-off are points of local extrema. Figure 17 shows the normal stress distributions at the mid-plane of the resin layers above and below the drop (dashed line above, solid below). Of particular interest is that for extensional loads, the resin is subjected to maximum compression and to maximum tension in the

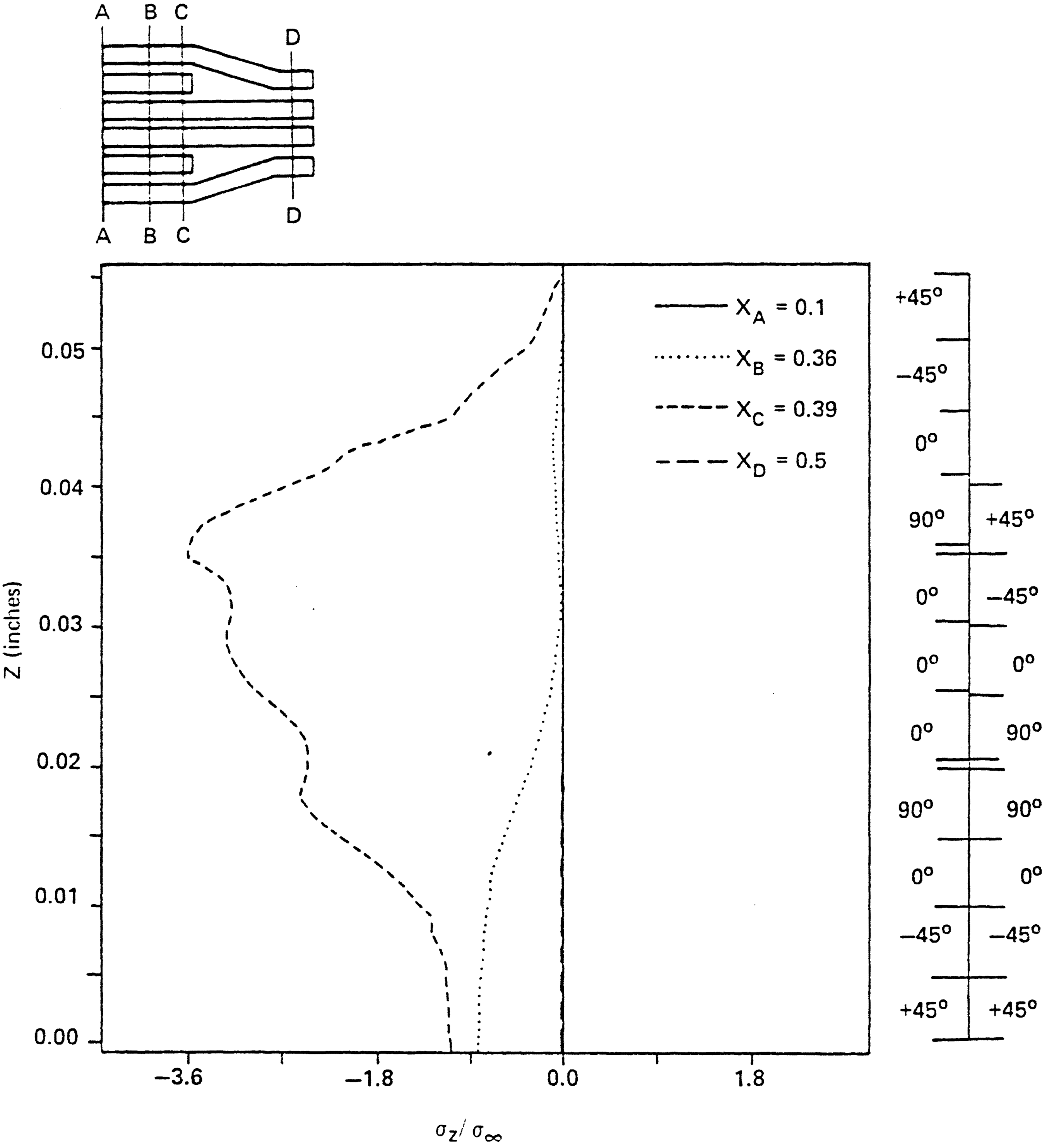

Fig. 15 Interlaminar normal stress variation through thickness for symmetric case.

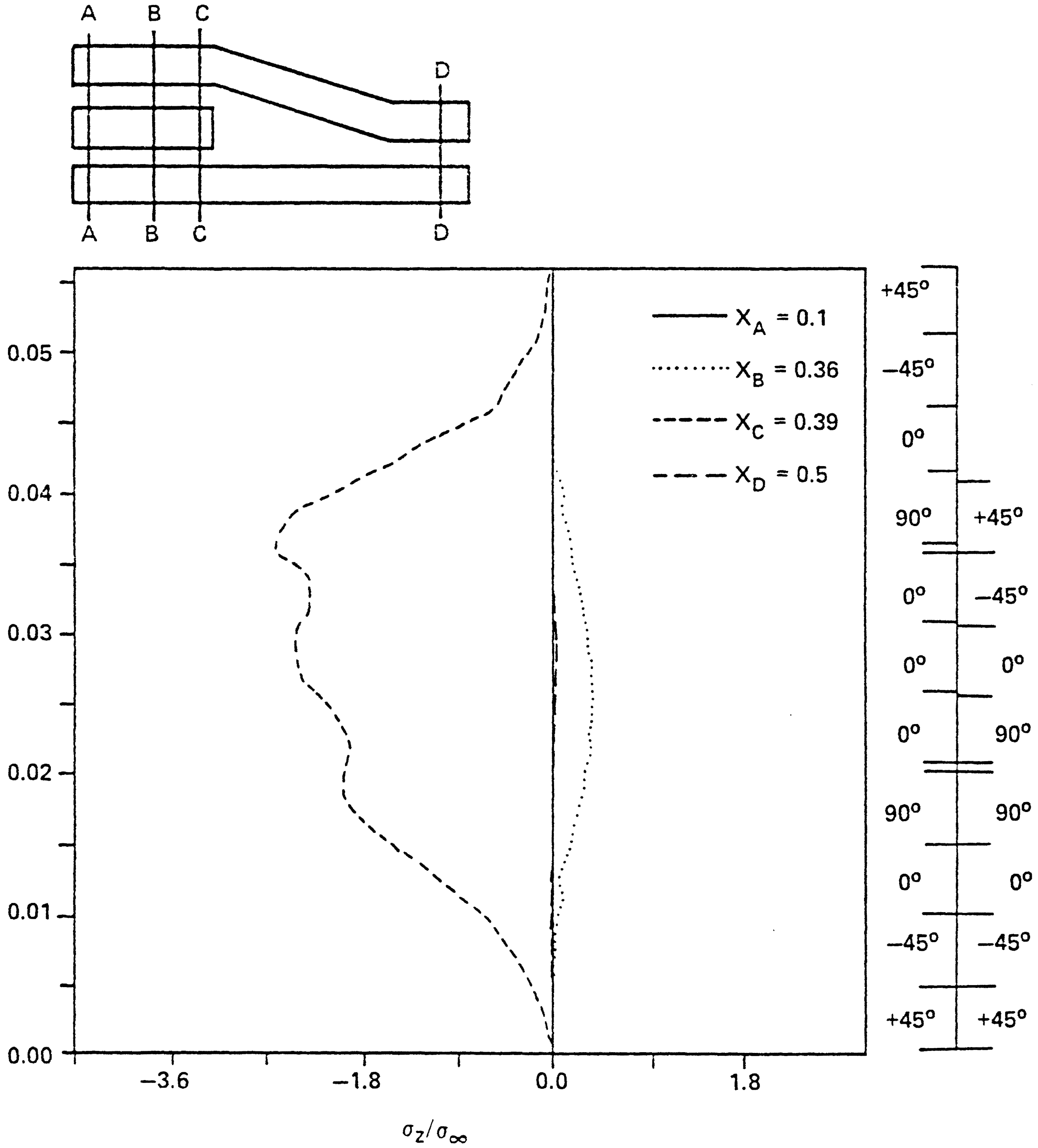

Fig. 16 Interlaminar normal stress variation through thickness for non-symmetric case.

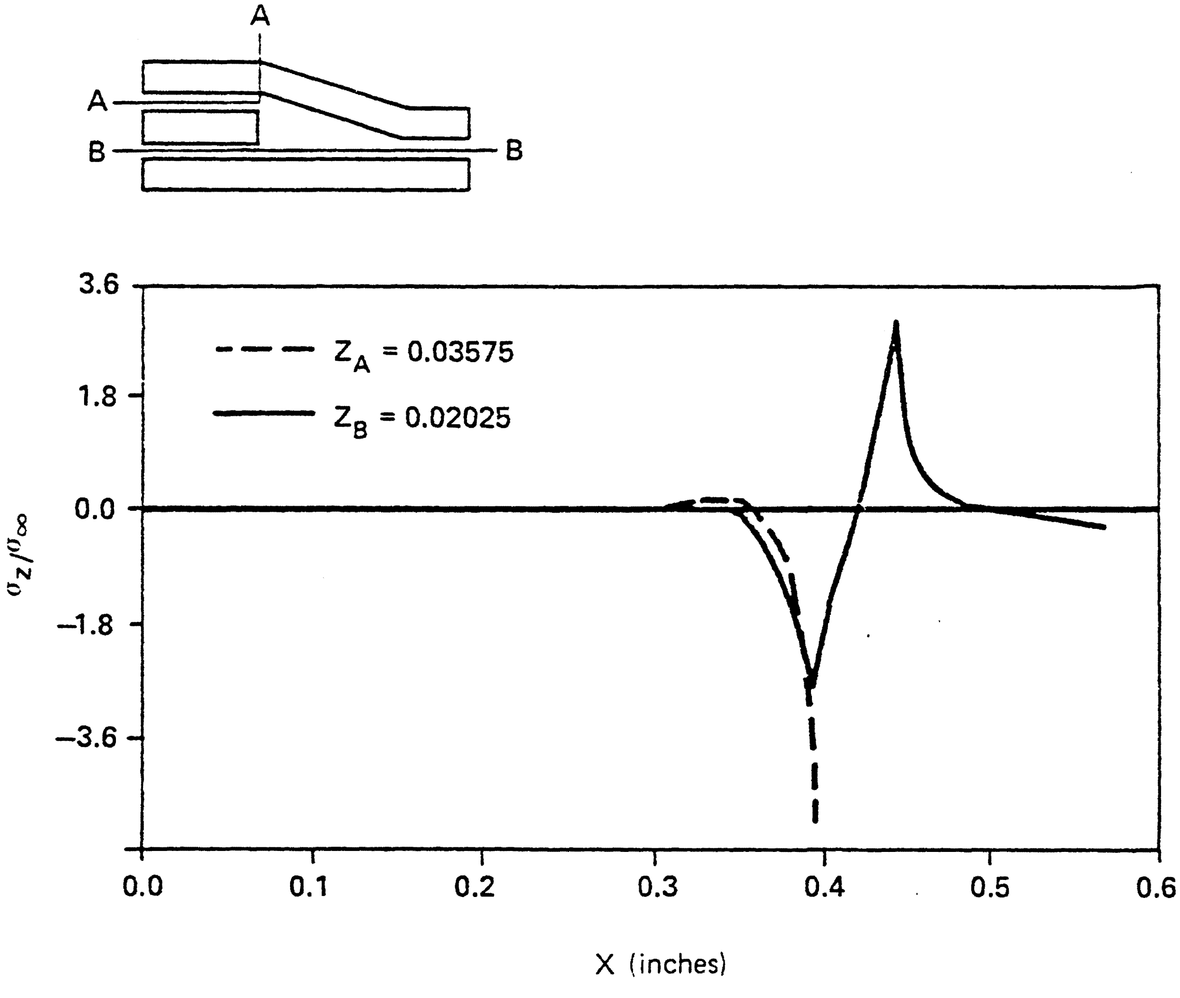

Fig. 17 Interlaminar normal stress variation along axis.

distance of the transition section in the lower interface. In all boundary and lay-up cases, the highest compression is at the drop in the upper interface. Also note the slight "undershoot" of the upper surface normal stress before vanishing in the far field. This positive region is the tensile normal stresses which is seen in Figure 16. The peak tensile value of interlaminar normal stress in the thick section is far below the peak compressive values for axial extensional loading.

Comparing Figure 17 to Figures 13 and 14, the distance required for the interlaminar normal stress to vanish is less than that required for interlaminar shear stress to vanish. The shear distances, therefore, govern the distance required to define the complete transfer of load.

In looking at the affects of parameter variations on the magnitudes of stress, again it is observed that the increase in number of plies dropped causes increases in peak normal stress values. The aspect ratio, however, has more influence over the normal stress than in previous stress components investigated. Increasing the aspect ratio from 3 to 6 can significantly decrease the normal stresses; even decreasing the normal stress peak more than an increase caused by increasing the number of dropped plies.

The laminate lay-up is also important, since the values of the interlaminar normal stress predicted for case 2 were all below those predicted for case 1.

3.4 Failure Predictions

The values of applied axial strain necessary for failure initiation were calculated for three separate modes of failure: resin failure, intralaminar tensile failure, and intralaminar compressive failure. As previously stated, the resin is assumed to be linear elastic until failure and, since the same strength is assumed in tension and compression, the failure strains presented in Table 4 are independent of the sign of axial loading.

As shown in Table 4, the location of failure initiation in the resin is in the upper interface at the ply drop-off for all the nonsymmetric cases and in one-half of the symmetric cases. For the remaining symmetric cases, resin failure initiated in the lower interface at the ply drop-off. At failure the stresses σ_x, σ_y, σ_z, and τ_{xz} are the major contributors to the resin failure, while the shear stresses τ_{yz} and τ_{xy} are three orders of magnitude less in the case 1 lay-up, and one order of magnitude less in the case 2 lay-up. The far field failure strain increases with increasing aspect ratio, which implies a less severe change in laminate thickness and an increasing volume of resin at the drop-off. In general the failure strain is less for the nonsymmetric conditions than for the symmetric conditions. Thus, the eccentric load path, which is represented by the nonsymmetric conditions, decreases the strain to failure for the resin failure mode. For a fixed aspect ratio and an increasing number of plies dropped, Table 4 shows mixed results on the failure strains. In the majority of cases the failure strain decreases as the number of plies dropped increases from one to two, then increases as the number of plies dropped increases from two to three. Hence, adding material to the laminate may not always increase the far field strain to failure; it depends on the relative influence of the stress concentration at the

Table 4

Applied Axial Strain for Resin Failure in µ in./in[*].

A. Case 1 Lay-up with Nonsymmetric Conditions

	Aspect Ratio			
n[**]	3	4	5	6
1	634	743	827	896
2	653	737	768	814
3	708	784	857	917

B. Case 1 Lay-up with Symmetric Conditions

	Aspect Ratio			
n	3	4	5	6
1	747	885	993	1079
2	828	934	955+	975+
3	867+	917+	958+	992+

C. Case 2 Lay-up with Nonsymmetric Conditions

	Aspect Ratio			
n	3	4	5	6
1	710	803	876	937
2	703	774	793	828
3	-	802	857	904

D. Case 2 Lay-up with Symmetric Conditions

	Aspect Ratio			
n	3	4	5	6
1	807	925	1014	1086
2	861	943	918+	939+
3	852+	885+	925+	959+

---

[*] All failures in upper interface at ply drop-off unless otherwise indicated.

[**] n equals the number of dropped 0^{o}-plies.

+Failure at the lower interface of the ply drop-off location.

drop-off. The exceptions to this trend occur for the case 2 lay-up, symmetric conditions, and for aspect ratios of three and four. In these cases the failure strain increases from one to two plies dropped, and then decreases from two to three plies dropped. The decrease in failure strain from two to three plies dropped appears to be due to a shift in failure location from the upper to lower interface. For comparative purposes, the strain to failure for a flat laminate identical to the thin section of the ply drop laminate is 9828 μ in/in for the resin failure mode. When comparing this value to the predicted resin mode failure strains in Table 4, it is apparent the ply drop causes significant stress concentration, which in turn decreases the far field strain to failure.

The first ply failures for the dropped ply must be separated for tensile and compressive loadings. The strengths of the material in the transverse plane are substantially different in tension and compression (see Table 1). The quadratic failure criterion (Equation 2.20) will therefore predict different magnitudes of failure initiation for tensile and compressive loading.

First ply failures due to applied tensile axial strains are shown in Table 5. The case 2 lay-up fails in the outermost ply (a 0^{o}-ply) at the reentrant corner in all cases examined and, as such, will not be discussed but is presented for completeness. For the case 1 lay-up the first ply failures occurred in the 90^{o}-ply adjacent to the top of the

Table 5

Applied Tensile Axial Strain for Intralamina Failure in μ in./in[*]

A. Case 1 Lay-up with Nonsymmetric Conditions

	Aspect Ratio			
n[**]	3	4	5	6
1	933	1081	1157	1223
2	946	1077	1151	1227
3	1020	1144	1198	1246

B. Case 1 Lay-up with Symmetric Conditions

	Aspect Ratio			
n	3	4	5	6
1	1008	1202	1300	1375
2	1060+	1241	1341	1400
3	1030+	1200+	1362	1376

C. Case 2 Lay-up with Nonsymmetric Conditions

	Aspect Ratio			
n	3	4	5	6
1	708#	999#	1230#	1412#
2	773#	1033#	1295#	1467#
3	753#	1009#	1256#	1429#

D. Case 2 Lay-up with Symmetric Conditions

	Aspect Ratio			
n	3	4	5	6
1	700#	986#	1211#	1384#
2	783#	1019#	1273#	1530#
3	773#	988#	1230#	1391#

---

[*] All failures in upper interface at ply drop-off unless otherwise indicated.

[**] n equals the number of dropped 0^{o}-plies.

+Failure in the ply adjacent to the upper interface at the reentrant corner.

#Failure in the outermost 0^{o} ply at the reentrant corner.

dropped plies. Within this 90^o-ply failure initiated at either the drop-off or at the axial location where the upper plies join the lower plies at the end of the transition section. Examination of the stresses at failure for case 1 revealed that σ_2, σ_3, and τ_{23} were major contributors to the failure criterion. For the case 1 lay-ups, the predicted strain to failure was always less for the non-symmetric case than the symmetric case. The eccentric load path represented by the non-symmetric boundary conditions decreases the tensile failure strain for the first ply failure of the case 1 lay-up. Similar results to the resin failures are predicted for variations in the number of plies dropped and the value of the aspect ratio; restated, a fixed aspect ratio and increasing number of plies dropped shows mixed results in Table 5. Also, increasing the aspect ratio for a fixed number of dropped plies always yields a higher predicted strain. Calculating a first-ply failure tensile strain for a flat laminate identical to the thin section of the ply drop laminate yields a value of 4202 μ in/in (a matrix tensile failure in the 90^oply).

Table 6 shows the calculated first-ply failures for a uniform compressive strain loading in the thin section. All compressive failures are predicted in the 0^o dropped plies at their termination point. The compressive failure strains are all larger in magnitude for the nonsymmetric boundary conditions than for the symmetric conditions. Most of the compressive failures are predicted at the top of the 0^o dropped plies, however, particularly in the nonsymmetric lay-ups, failure location is moved to the bottom of the dropped plies for

Table 6

Applied Compressive Axial Strain for Intralamina Failure in μ in./in[*]

A. Case 1 Lay-up with Nonsymmetric conditions

	Aspect Ratio			
n[**]	3	4	5	6
1	-1077	-1177	-1273	-1353+
2	-1099	-1241+	-1326+	-1410+
3	-1177+	-1325+	-1412+	-1466+

B. Case 1 Lay-up with Symmetric Conditions

	Aspect Ratio			
n	3	4	5	6
1	-1001	-1065	-1130	-1187
2	-887	-990	-1099	-1193
3	-875	-996	-1103	-1192

C. Case 2 Lay-up with Nonsymmetric Conditions

	Aspect Ratio			
n	3	4	5	6
1	-1038	-1119	-1205	-1282
2	-1004	-1163	-1329	-1443+
3	-1160#	-1311	-1450#	-1515#

D. Case 2 Lay-up with Symmetric Conditions

	Aspect Ratio			
n	3	4	5	6
1	-983	-1037	-1099	-1158
2	-851	-955	-1071	-1164
3	-1035#	-960	-1071	-1166

---

[*] Failure at the top of the dropped 0^o-plies at drop-off unless otherwise indicated

[**] n equals the number of dropped 0^o-plies.

+Failure at the bottom of the dropped 0^o-plies at location of drop-off.

#Failure in the center portion of the dropped 0^o-plies at location of drop-off.

the higher drops and aspect ratios. Again, this change in location is attributed to the increase in load path eccentricity. In the dropped plies, the in-plane stresses are small in comparison to the through-the-thickness stresses at the drop-off. Thus, the stresses σ_3, σ_{23}, and some σ_2 in the dropped 0^o plies are the major contributors to the first-ply failure criterion. The compressive failure strain for a flat laminate identical to the thin section of the ply drop laminate is -18,556 μ in/in for the first ply failure mode (failure in a 0^o ply). The significant reduction in the compressive strain to failure for the ply drop laminate is due to the through-the-thickness stresses generated at the drop-off.

Considering the three failure modes simultaneously, the first failure event in either tension or compression is a resin failure except in a few cases. The few exceptions are the tension first ply failures for the case 2 lay-up with an aspect ratio of 3, where failure occurred at the reentrant corner.

Collecting the predictions of failure for the dropped ply configuration exemplifies the complexity in analyzing composite materials. For the identical geometry, a completely isotropic material predicts stress concentrations always at the reentrant corner as a function of the angle of opening.

CHAPTER IV

DISCUSSION AND CONCLUSIONS

The response of a graphite-epoxy laminate containing terminating internal plies has been examined. The change in laminate thickness due to the terminated plies causes complex stress distributions in the vicinity of the ply drop. Based on microphotographs (Figures 3 and 4) of laminates fabricated with ply drop-offs, a linear elastic finite element analysis was performed on an idealized approximation of the ply drop geometry.

The modeling procedure used assumed a step change in the slope of the fiber planes in the upper plies in the transition section. For geometric compatability with the upper plies in the thick and thin sections, the lamina thickness in the upper plies in the transition section is decreased by the cosine of the slope angle. Thus, the lamina in the upper plies of the transition section would have increased fiber volume fractions. This effect was also neglected. If the lamina thickness were kept constant, then more complicated modeling techniques must be used where the upper plies meet at each end of the transition section.

The approximations to the actual geometry also included a pocket of pure resin adjacent to the dropped plies and resin-rich regions between the dropped plies and the remaining laminate. The size of the resin pocket is determined by the number of plies dropped and the slope of the plies encasing the dropped plies from above.

A parametric study on the affects of two different lay-ups, symmetric and nonsymmetric lower surface boundary conditions, number of plies dropped, and aspect ratio of the triangular resin pocket in front of the drop-off, on the response and failure were examined. The applied loads at the end of the thin section result in either uniform extensional or compressive axial strain. The symmetric lower surface boundary conditions result in a concentric load path, whereas the nonsymmetric lower surface conditions (traction free) result in an eccentric load path.

The analysis shows that the in-plane stresses in the dropped plies are small with respect to the through-the-thickness stresses at the drop-off; for an axial force applied to the laminate beyond the dropped plies the load is transferred to the terminated plies by shear rather than through the ends of the dropped ply fibers. In regions adjacent to the dropped plies, modeled by a thin resin-rich layer, the interlaminar stresses are the same order of magnitude as the in-plane normal stresses. Interlaminar stresses are largest at the ply drop-off (as much as eight to ten times the applied load in the resin), decrease in an exponential manner with increasing axial distance from the drop-off, and vanish in the far field. For one ply dropped, the axial distance required for the interlaminar stresses to vanish is approximately 20h, where h denotes the ply thickness. For each additional ply dropped, the additional axial distance required for the interlaminar stresses to vanish is about 5h. The aspect ratio did not have a great affect on the shearing distance for a constant number of dropped plies. In regions of the laminate where the interlaminar stresses vanish, the state of stress is planar and classical lamination theory is applicable.

Results of the parametric study were also used to predict the location and magnitude of applied strains at the initiation of failure. The linear elastic analysis of the ply drop configuration subject to tension or compression indicates that failure initiates at the resin interfaces surrounding the dropped plies in all but a few cases. The few exceptions are tension first-ply failures in a 0° ply at the reentrant corner. Failure initiation was typically predicted for applied far-field strains on the order of 1000 μ in/in.

With the exception of the laminates which failed at the reentrant corner, there were minor differences in the applied strain at failure for the two lay-ups studied. For the resin failures, there was a reduction in the load carrying capacity of the nonsymmetric structure because of bending loads. However, for both the symmetric and nonsymmetric boundary conditions, the far field failure strain increased monotonically as the aspect ratio was increased from 3 to 6.

Also, in a majority of cases the applied strain to failure decreases for one to two drops and slightly increases for two to three drops. Thus adding material to the laminate does not always increase the far field strain to failure.

The finite element computer code which was developed for this analysis provides the capacity to solve large static problems by using efficient storage schemes. The problem size is limited only by available on-line computer storage or computer funds. The only modification desirable would be the inclusion of an element which smears several lamina into a single layer particularly in regions far from the ply drop where lamination theory applies. Though not specifically designed for this purpose, the versatility of material inputs could be used to achieve this goal, however, such procedures would causes extensive changes in the input files.

The above modifications would be incorporated into the mesh generation program which was written to automatically generate ply configurations with or without dropped plies or zones of mesh refinement. The combined use of these programs will greatly reduce the effort required to analyze other laminate configurations.

Although more analytical work could be done, the model used here should be verified with experimental studies. In addition to experimental work some effort should be placed on discerning the affect the manufacturing process has on the ply drop configuration. The microphotographs showed that there was a visible increase in the fiber volume fraction of the plies near the resin pocket. Finally, a future study might include the effect of material nonlinearity. The pure resin pocket, in addition to possible poor bond quality or voids, has the lowest strength and is easily loaded beyond its proportional limit. The extent of the plastic zone will affect load transfer to the dropped plies in the region of high shear strain.

REFERENCES

1. Jones, R. M., Mechanics of Composite Materials, McGraw-Hill, New York, 1975, pp. 232-234, 40-41, 147-156, 80-82.

2. Schwartz, M. M., Composite Materials Handbook, McGraw-Hill, New York, 1984, pp. 3.20-3.21.

3. Wilkins, D. J., "A Preliminary Damage Tolerance Methodology for Fibrous Composite Structures", compiled by Ahmed K. Noor, Mark J. Shuart, James H. Starnes, Jr., and Jerry G. Williams, NASA Conference Publication 2278, 1983, pp 67-93.

4. Adams, D. F., Ramkumar R. L. and Walrath D. E., "Analysis of Porous Laminates in the Presence of Ply Drop-Offs and Fastener Holes", Northrop Technical Report NOR 84-113, Northrop Corp., Hawthorn, CA, and University of Wyoming, Laramie, Wyoming, May 1984.

5. Pipes, R. B., and Pagano, N. J., "Interlaminar Stresses in Composite Laminates Under Uniform Axial Extension", Journal of Composite Materials, Vol. 4, October 1970, pp 538-548.

6. Hsu P. W., and Herakovich C. T., "Edge Effects in Angle-Ply Composite Laminates", Journal of Composite Materials, Vol. 11, October 1977, pp 422-428.

7. Wang, S. S. and Stango, R. J., "Optimally Discretized Finite Elements for Boundary Layer Stresses in Composite Laminates", AIAA Journal, Vol. 21. No. 4, April 1983, pp 614-620.

8. Lekhnitskii, S.G., Theory of Elasticity of an Anistropic Body, Holden-Day, San Francisco, 1963, p.129.

9. Goland, M., and Reissner, "The Stresses in Cemented Joints", Journal of Applied Mechanics, March 1944, pp A17-A27.

10. Hart-Smith, L. J. "Adhesive-Bonded Single-Lap Joints", NASA CR-112236, January 1973.

11. DOD/NASA Advanced Composites Design Guide, Structures/Dynamics Division AFWAL/FDL, Wright-Patterson Air Force Base, Ohio, July 1983, Vol. 1, Section 1.1.3 and 1.3.

12. Cope, R. D., and Pipes R. B., "Design of the Composite Spar-Wingskin Joint", Composites, January 1982, pp 47-53.

13. Knight, M. and Pagano N. J., "The Determination of Interlaminar Moduli of Graphite/Epoxy Composites", Seventh Annual Mechanics of Composites Review, AFWAL/NASA/NAVY/ARMY, Dayton, Ohio, October 1981.

14. Herakovich, C. T., Nagarka, A., and O'Brien, D. A., "Failure Analysis of Composite Laminates with Free Edges", *Modern Development in Composite Materials*, J. R. Vinson editor, ASME, 1979, pp. 53-66.

15. Bathe, K. J. and Wilson, E. L., *Numerical Methods in Finite Element Analysis*, Prentice Hall, Englewood Cliffs, New Jersey, 1976, p. 25, 32.

16. Mondkar D. P. and Powell G. H., "Large Capacity Equation Solver for Structural Analysis", *Computer and Structures*, Vol. 4, 1974, pp. 699-728.

17. Pagano, N, J., "Influence of Shear Coupling in Cylindrical Bending of Anistropic Laminates", *Journal of Composite Materials*, 1970, pp. 330-341.

18. Statistical Analysis Systems, Inc., SAS/GRAPH Enhancements and Updates for 82.2 release, SAS Technical Report p. 121, October 10, 1982, SAS Inst. Inc., pp. 56-63.

Appendix A

In a series of papers, Pagano et al, [17] have investigated the range of applicability of classical laminated plate theory under static bending. Exact elasticity solutions are obtained for the problem of a pinned-end laminate under cylindrical bending. These solutions have indicated rather wide discrepancy between the classical theory and the exact elasticity solution for laminates having low span-to-depth ratios.

In the range of span-to-depth ratios where classicial theory inaccurately represents laminate response numerical solutions will be tabulated comparing the solutions of various finite element meshes to an exact elasticity solution. The numerical results presented are for a four ply antisymmetric angle-ply laminate with a span-to-depth ratio of four. The ply orientations are (+30, -30, +30, -30), all ply thicknesses are h, and the body is subjected to a half-sine normal traction on the upper surface. The material properties used for the comparison are

$$E_1 = 25.0 \times 10^6 \text{ psi}$$

$$E_2 = E_3 = 1.0 \times 10^6 \text{psi}$$

$$G_{12} = G_{13} = 0.5 \times 10^6 \text{ psi}$$

$$G_{23} = 0.2 \times 10^6 \text{ psi}$$

$$V_{12} = V_{13} = V_{13} = 0.25$$

$$h = 0.005 \text{ inches}$$

The finite element calculations are presented for two cases. Each case has one element through the thickness of each ply, while having one and four elements spanning the half length of the laminate (hence referred to as Case A and Case B respectively).

The displacements are the primary solution variables. The exact solution displacements vary exponentially through the thickness and sinusoidally along the span, the finite element displacements vary quadratically within an element. The following table summarizes the element capability to predict elasticity solutions.

Displacement Component	Exact Solution	Case A disp(%error)	Case B disp(%error)
u max x 10^{-8}	3.253	3.343 (2.7)	3.236 (0.5)
u min x 10^{-8}	-3.292	-3.393 (3.1)	-3.276 (0.5)
w . midplane x 10^{-7}	1.685	1.663 (1.3)	1.678 (0.4)

The stresses are the secondary solution variables. All stress components are appreciably underestimated by classical plate theory. The following table summaries the capability to predict the highest value of various stress components.

Stress Component	Exact Solution	Case A disp (Δ%)	Case B disp (Δ%)
σ_x max	13.621	14.53 (6.7)	13.69 (0.5)
τ_{xz} max	2.03	2.63 (29.6)	2.25 (10.8)
τ_{xy} max	5.58	5.85 (4.8)	5.61 (0.5)
τ_{yz} max	0.51	0.77 (51.0)	0.62 (21.5)
σ_z max	1.00	1.066 (6.6)	1.035 (3.5)

The vita has been removed from
the scanned document

RESPONSE AND FAILURE ANALYSIS OF A GRAPHITE-EPOXY LAMINATE CONTAINING TERMINATING INTERNAL PLIES

by

Brian Lee Kemp

(ABSTRACT)

A change in laminate thickness due to terminating internal plies acts as a stress riser for both intralamina and interlaminar stresses. This laminate configuration is referred to as a ply drop. The linear elastic, three-dimensional stress distributions in the vicinity of a ply drop are determined for a graphite-epoxy laminate subject to axial tension and compression by a finite element analysis. It is shown that the interlaminar stresses have a maximum magnitude at the ply drop-off, and decrease proceeding away from the drop-off. Two modes of failure initiation are analyzed. In the pure resin regions surrounding the dropped plies, the maximum stress criterion is assumed to govern failure. The Tsai-Wu criterion is used for intralamina failure prediction. The influence of two laminate lay-ups and a variety of ply drop geometries on the response and failure are presented.